

A new formation model for ω Centauri: the crossroad of astrophysical processes

Kenji Bekki

*ICRAR, M468, The University of Western Australia 35 Stirling Highway, Crawley
Western Australia, 6009, Australia*

and

Takuji Tsujimoto

National Astronomical Observatory of Japan, Mitaka, Tokyo 181-8588, Japan

ABSTRACT

We investigate the formation processes of the Galactic globular cluster (GC) ω Cen with multiple stellar populations based on our original hydrodynamical simulations with chemical enrichment by Type II supernovae (SNe II), asymptotic giant branch (AGB) stars, and neutron star mergers (NSMs). Multiple stellar populations with a wide range of $[\text{Fe}/\text{H}]$ can be formed from rather massive and compact molecular cloud with a mass of $\approx 2 \times 10^7 M_{\odot}$ in the central region of its dwarf galaxy within less than a few hundred Myr. Gas ejected from SNe II and AGB stars can mix well to form new stars with higher He abundances (Y) and higher $[\text{Fe}/\text{H}]$. The He-rich stars are strongly concentrated in the GC's central region so that the GC can show a steep negative gradient of Y . Relative ratios of light elements to Fe show bimodal distributions for a given $[\text{Fe}/\text{H}]$ owing to star formation from original gas and AGB ejecta. $[\text{La}/\text{Fe}]$ and $[\text{Ba}/\text{Fe}]$ can rapidly increase until $[\text{Fe}/\text{H}] \sim -1.5$ and then decrease owing to Fe ejection from SNe II. Although AGB ejecta can be almost fully retained in intra-cluster medium, NSM ejecta can be retained only partially. This difference in the retention capability is responsible for the observed unique $[\text{Eu}/\text{Fe}] - [\text{Fe}/\text{H}]$ and $[\text{La}/\text{Eu}] - [\text{Fe}/\text{H}]$ relations in ω Cen. The observed $[\text{O}/\text{Na}] - [\text{Fe}/\text{H}]$ relation and radial $[\text{Fe}/\text{H}]$ gradient are yet to be well reproduced in the present model. We briefly discuss how the results change for different yields of AGB stars and SNe II.

Subject headings: The Galaxy, globular clusters, chemical abundances

1. Introduction

The formation of globular clusters (GC) with multiple stellar populations is the cross-road of various astrophysical processes. It involves, for example, long-term dynamical evolution driven by two-body relaxation (e.g., Vesperini et al. 2010), dynamical influences of the Galactic disk (e.g., Gnedin et al. 1999), mixing of intra-cluster medium (ICM) with gas ejected from fast-rotating massive stars (e.g., Prantzos & Charbonel 2006) and from asymptotic giant branch (AGB) stars (e.g., D’Antona & Ventura 2002), secondary star formation within existing dense stellar systems (e.g., D’Ercole et al. 2008), enrichment of r -process elements due to efficient retention of gaseous ejecta from neutron star mergers (NSMs) in high-density ICM (Bekki & Tsujimoto 2017; BT17), and stellar nucleosynthesis (e.g., Renzini et al. 2015). It is crucial for any theoretical study of GC formation to understand the relative importance of each of these processes in the formation of their multiple stellar populations. However, no theory has so far explained the observed various properties of their multiple stellar populations in a self-consistent manner (e.g., see Bastian & Lardo 2018 for a recent review).

The Galactic GC ω Cen is a unique laboratory to study physical processes related to the origin of multiple stellar populations of GCs, because there are so many previous observational studies on chemical and dynamical properties of ω Cen. It is observed to have characteristic features such as its large mass and flattened shape (e.g., Meylan 1987; Meylan et al. 1995), possibly different kinematics in different stellar populations (e.g., Norris et al. 1997; Bellini et al. 2018), large metallicity dispersion (e.g., Freeman & Rodgers 1975; Norris et al. 1996), different spatial distributions among multiple stellar populations (e.g., Pancino et al. 2000; Ferraro et al. 2002), possible age spreads among the populations (e.g., Lee et al. 1999; Smith et al. 2000, S00; Marino et al. 2011); retrograde orbit with respect to the Galactic rotation (e.g., Dinescu et al. 1999), double main sequence in the color magnitude diagram (e.g., Anderson 1997; Bedin et al. 2004), large spread in helium abundance Y (e.g., Piotto et al. 2005), and radial gradient of Y (e.g., Sollima et al. 2007). Recent observations of color magnitude relations of ω Cen have identified 15 subpopulations with possibly different chemical abundances in ω Cen (e.g., Bellini et al. 2017). Different theoretical models for ω Cen have tried to provide physical explanations for these unique characteristics of ω Cen (e.g., Carraro & Lia 2000; Bekki & Freeman 2003, BF03; Tsujimoto et al. 2003).

One of promising scenarios for the formation of ω Cen is that it had been the nucleus of a dwarf galaxy that was completely destroyed by the early formation phase of the Galaxy (e.g., Freeman 1993). Dynamical evolution of a nucleated dwarf galaxy into a naked nucleus (i.e., ω Cen) has been investigated in details by several authors (e.g., BF03; Mizutani & Chiba 2003; Igeta et al. 2005). For example, BF03 demonstrated that (i) a large amount

of more metal-rich gas can be transferred into the nucleus of a gas-rich nucleated dwarf and (ii) the nucleus can therefore have multiple generation of stars with different metallicities. Previous observations discovered possible tidal debris from ω Cen (e.g., Wylie de-Boer et al. 2010) and recent observations of the Galactic halo stars based on Gaia data have revealed the evidence of stellar streams kinematically associated with ω Cen (e.g., Myeong et al. 2018; Ibata et al. 2019). These observations imply that the above formation scenario of ω Cen is promising.

Although dynamical origins of ω Cen have been extensively discussed so far, its chemical properties have not been modeled in detail. Ikuta & Arimoto (2000) adopted the self-enrichment scenario of ω Cen and thereby investigated how the initial mass function of stars (IMF) and gaseous outflow and inflow during the early evolution of ω Cen can control the distribution of $[\text{Ca}/\text{H}]$ in ω Cen. Using one-zone chemical evolution models of ω Cen, Romano et al. (2007) tried to reproduce the observed abundance distribution function (ADF), age-metallicity relation (AMR), and $[\text{Fe}/\text{H}]-[\alpha/\text{Fe}]$ relation. They modeled a long-term (~ 3 Gyr) star formation history in order to reproduce the possibly decreasing $[\alpha/\text{Fe}]$ and increasing $[\text{Cu}/\text{Fe}]$ with increasing $[\text{Fe}/\text{H}]$ (for $-2 \leq [\text{Fe}/\text{H}] \leq -0.3$) in ω Cen. Marcolini et al. (2007) investigated the long-term (~ 1.5 Gyr) evolution of ω Cen based on 3D hydrodynamical evolution with feedback effects of SNe II and SNe Ia on ICM. Although they reproduced the overall metallicity spread observed in ω Cen, they failed to explain its Y spread. These previous models assumed that star formation can last more than ~ 1 Gyr in the formation of ω Cen.

Recent observations have found, however, that there appears to be no/little change in $[\text{Si}/\text{Fe}]$ and $[\text{Ca}/\text{Fe}]$ in stellar populations of ω Cen (Johnson & Pilachowski 2010, JP10; Magurno et al. 2019). Since chemical enrichment by SNe Ia can decrease $[\alpha/\text{Fe}]$ with increasing $[\text{Fe}/\text{H}]$, the observed lack of $[\alpha/\text{Fe}]$ evolution with $[\text{Fe}/\text{H}]$ has been suggested to be no/little chemical enrichment of ICM by SNe Ia in ω Cen (JP10). These observations therefore imply that star formation should be completed within an order of 10^8 yr, because some fraction of SNe Ia promptly enrich ICM within 1 Gyr (Totani et al. 2008). Such a short formation timescale is inconsistent with most of previous works for the ages of stellar populations in ω Cen: see Table 1 for a summary of these works. D’Antona et al. (2011) have investigated correlation/anti-correlation between $[\text{O}/\text{Fe}]$ and $[\text{Na}/\text{Fe}]$ among stars with $[\text{Fe}/\text{H}]$ ranging from -2 to -0.3 in ω Cen (see their Fig. 1) and concluded that the formation timescale of ω Cen should be a few times 10^8 yr: the observed O and Na abundances matches well with yields from massive AGB stars (not from low-mass ones). These recent results are inconsistent with the long star formation timescale adopted in previous theoretical works. Thus, a new model needs to be constructed that can self-consistently explain these recent observations as well as previous observations.

The purpose of this paper is thus to investigate chemical and dynamical evolution of ω Cen in its early formation history based on a new model of ω Cen. In the new model, ω Cen was formed from a giant molecular cloud (GMC) in the central region of its host dwarf galaxy that is a building block of the Galaxy. Almost all stars of ω Cen are formed from multiple episodes of star formation within ~ 300 Myr so that $[\alpha/\text{Fe}]$ of the stars ($\alpha=\text{Si}$, Ca , and Ti , not O and Mg) can be kept high (higher than the solar value). Chemical enrichment in ω Cen can proceed rapidly, because SNe II from multi-generations of stars can pollute the ICM very efficiently. Gas ejected from AGB stars and NSM can be mixed with ejecta from SNe II, which ended up with the formation of stars with high Y and with large variations in r - and s -process elements.

The plan of the paper is as follows. We describe the models of ω Cen formation in a dwarf galaxy in §2. We present the results of chemical evolution of forming ω Cen in §3. Based on these results, we provide several implications of the results and discuss how well the new model can reproduce the existing observations in §4. We summarize our conclusions in §5. Our previous works already discussed the formation of ω Cen from a nucleated dwarf galaxy (BF03), dynamical evolution of multiple cluster systems formed from GMCs (Bekki 2017; B17a), and GC formation within massive fractal GMCs (Bekki 2017b; B17b). We therefore focus exclusively on the chemical properties of ω Cen and their spatial variations in the present study. We only focus on the chemical evolution of 12 elements (H , He , C , N , O , Na , Mg , Al , Fe , Ba , La , and Eu) and does not discuss extensively other elements such as Pb and Mn in the present study though these abundances have also fossil information on the chemical evolution of ω Cen (e.g., Cunha et al. 2010; D’Orazi et al. 2011, D11; Romano et al. 2011; Pancino et al. 2011).

2. The model

2.1. Overview

In the present formation scenario of ω Cen, a metal-poor ($[\text{Fe}/\text{H}] \sim -1.7$) GMC with the total mass of $\sim 10^7 M_\odot$ was first formed in the central region of a gas-rich dwarf galaxy that was a building block of the Galaxy. Accordingly, the GMC was initially surrounded by low-metallicity ($[\text{Fe}/\text{H}] < -1.7$) field stars, a fraction of which was later gravitationally bound by ω Cen to be metal-poor stars with $-2.2 < [\text{Fe}/\text{H}] < -1.7$ observed in ω Cen (e.g., Rey et al. 2000; JP10; Bono et al. 2019). Although the formation process of such a very massive GMC is not specified in the present study, tidal interaction of the dwarf with the Galaxy could be responsible for the formation of such a GMC. After the initial bursty formation of first generation (1G) stars within the GMC, a large number of SNe II can expel the significant amount of gas left over from the burst. Gas ejected from 1G AGB ejecta can be trapped by the deep potential well of the host dwarf so that second generation (2G) of stars can be formed from the gas. The ejecta of SNe II from 2G population can be trapped in the central region of the dwarf and consequently mixed with gas ejected from 1G AGB stars to form third generation of stars. External accretion of pristine gas from interstellar medium (ISM) onto ω Cen for mixing with AGB ejecta is not considered in the present study, though such accretion is a key process in the formation of other massive GCs like Terzan 5 (e.g., McKenzie & Bekki 2018) and 47 Tuc (McKenzie & Bekki 2019, in preparation).

Gas ejected from NSMs can be trapped by the ICM when a large amount of AGB ejecta is accumulated in the central region of 1G stars, because the ejecta from NSMs can lose energy and momentum through interaction with the high-density ICM (see BT17 for discussion on this point). Accordingly, AGB ejecta is crucial for the formation of new stars from gas polluted by NSM in the present scenario. Although NSM ejecta can significantly increase $[\text{Eu}/\text{Fe}]$ in the ICM, SNe II ejecta from later generations (LG) of stars can decrease $[\text{Eu}/\text{Fe}]$. Therefore, NSM events in LG need to be incorporated in the present chemodynamical model so that the observed flat $[\text{Eu}/\text{Fe}]$ – $[\text{Fe}/\text{H}]$ relation can be reproduced. The formation of new stars from AGB and NSM ejecta mixed with SNe II ejecta can continue over ~ 300 Myr until AGB ejecta is expelled either by SNe Ia or by ram pressure stripping by the Galactic warm/hot gas. During the destruction of the host dwarf, the initially massive ω Cen can lose a significant fraction of its 1G stars to the early Galactic halo. We neither model the truncation of star formation by SNe Ia or ram pressure nor investigate the destruction process of the host dwarf in the present study.

The present study does not discuss the origin of metal-poor stars with ($[\text{Fe}/\text{H}] < -1.7$) observed in ω Cen (JP10) in a quantitative manner. We consider a scenario in which these

metal-poor stars existed before the formation of the natal GMC of ω Cen and were gravitationally trapped by ω Cen after its formation. Our previous simulations of nucleated dwarfs showed that a minor fraction of field stars around stellar nuclei/nuclear star clusters can be still gravitationally trapped by the nuclei/clusters even after the destruction of their host dwarfs (Bekki & Yong 2012). Therefore, the above scenario can be regarded as quite convincing and realistic. We use our own original simulation code that can be run on GPU clusters (Bekki 2013a) in order to perform smooth particle hydrodynamics (SPH) simulations of GC formation within massive MCs.

2.2. Fractal GMC

Since the details of fractal GMC models adopted in the present study are given in B17b, we here briefly describe the models. A GMC with a size R_{gmc} and a mass M_{gmc} is assumed to be represented by $\sim 10^6$ SPH particles and have fractal structures within it. A GMC is assumed to have a power-law radial density profile ($\rho_{\text{gmc}}(r)$) as follows:

$$\rho_{\text{gmc}}(r) = \frac{\rho_{\text{gmc},0}}{(r + c_{\text{gmc}})^\beta}, \quad (1)$$

where r , $\rho_{\text{gmc},0}$, and c_{gmc} , β are the distance from the GMC's center, a constant that is determined by M_{gmc} and R_{gmc} , the core radius of the GMC, and the power-law slope, which is fixed at 1 in the present study. The GMC is assumed to have a fractal gaseous distribution characterized by a fractal dimension D_3 that is fixed at 2 in the present study.

The initial virial ratio (t_{vir}) of a GMC is described as follows:

$$t_{\text{vir}} = \frac{2T_{\text{kin}}}{|W_{\text{gmc}}|}, \quad (2)$$

where W_{gmc} is the initial total potential energy of the GMC and T_{kin} is the total kinetic energy due to random motion and global rotation in the GMC. We present only the results of the models with $t_{\text{vir}} = 0.4$. We also consider rigid rotation of a GMC in some models, because previous observations suggested that velocity gradients within MCs could be due to such rotation (e.g., Phillips 1999; Rosolowsky et al. 2003). Accordingly, T_{kin} is the combination of the total random energy T_{ran} and the total rotational one (T_{rot}), and the ratio of the two (f_{rot}) is a parameter in the present study as follows:

$$f_{\text{rot}} = \frac{T_{\text{rot}}}{T_{\text{kin}}}. \quad (3)$$

We mainly show the results of the models with $f_{\text{rot}} = 0.01$ in the present study, because recent observations show that the angular momentum of GMCs is quite small (e.g., Rosolowsky et

al. 2003). We also investigate the models with different f_{rot} to understand how f_{rot} changes the structure and kinematics of ω Cen. Initial gaseous temperature and metallicity are set to be 10K and $[\text{Fe}/\text{H}]=-1.7$ in all MCs. The early chemical enrichment and feedback effects in natal GMCs by stellar winds of OB stars (e.g., Bekki & Chiba 2007) are not included in the present study.

2.3. Host dwarf

The most important role of ω Cen’s host dwarf is that its deep gravitational potential can retain gas ejected from stars during the intense star formation. Since the host dwarf should be dominated by dark matter, we only consider the mass distribution of dark matter. We adopt the density distribution of the NFW halo (Navarro, Frenk & White 1996) derived from Λ CDM simulations in order to describe the radial mass density profile of a dark matter halo in a disk galaxy as follows:

$$\rho(r) = \frac{\rho_0}{(r/r_s)(1 + r/r_s)^2}, \quad (4)$$

where r , ρ_0 , and r_s are the spherical radius, the characteristic density of a dark halo, and the scale length of the halo, respectively. The c -parameter ($c = r_{\text{vir}}/r_s$, where r_{vir} is the virial radius of a dark matter halo) and r_{vir} are chosen appropriately as 16 for the low-mass dwarf with the total mass of $10^{10}M_{\odot}$ and $r_s = 1.2$ kpc.

2.4. Star formation

We consider that if the mass density of a gas particle (ρ_g) is higher than the threshold gas density for star formation ($\rho_{g,\text{th}}$), then the gas particle is converted into a new stellar particle. Therefore, the physical condition for star formation is as follows:

$$\rho_g > \rho_{g,\text{th}}. \quad (5)$$

Since the typical mass density of the core of a GMC is 10^5 atom cm^{-3} (e.g., Bergin & Tafalla 2007), we adopt $\rho_{g,\text{th}} = 10^5$ atom cm^{-3} as a reasonable value. In the present study, we consider that the IMF can be different between new stars formed from original gas of a GC-forming GMC (1G stars) and those formed from gas ejected from 1G stars (2G stars). This is mainly because our recent simulations have demonstrated the IMF in 2G star formation to be more top-light (i.e., a smaller number of SNe II progenitors) owing to dynamical influences of existing dense stellar systems on gas from 1G stars (Bekki 2019a, B19a). 1G

stars are assumed to have the canonical Salpeter IMF with the slope of -2.35 and the lower-mass and upper-mass cutoffs being $0.1M_{\odot}$ and $50M_{\odot}$, respectively. This might not be a reasonable choice, because our previous simulations showed that the IMF can be top-heavy in the nuclear starburst regions of galaxies (Bekki 2013b), which could be relevant to the formation site of ω Cen in the present study. However, we use the canonical IMF and discuss the problem of this IMF in reproducing the observed properties of ω Cen in §4.

2G stars are assumed to have the top-light IMF with the slope of -2.35 and the mass fraction of SNe II (f_{sn2}) for 2G stars being 0.02 in all models of the present study. This f_{sn2} is by a factor of 7 smaller than that for 1G stars. We have investigated the models with different f_{sn2} in order to find the best model for ω Cen in which the maximum $[\text{Fe}/\text{H}]$ in the stars can be as large as -0.3 . We have found that f_{sn2} should be as low as 0.02, because the models with larger f_{sn2} shows the maximum $[\text{Fe}/\text{H}]$ larger than 0. Also, the adopted models with the top-light IMF means weaker SNe II feedback effects thus a larger amount of ICM being converted into new stars. Thus, we describe the results mainly for the models with $f_{\text{sn2}} = 0.02$ in the present study.

2.5. Chemical enrichment

2.6. Chemical yields

In the present study, we investigate the time evolution of chemical abundances of 12 elements, H, He, C, N, O, Na, Mg, Al, Fe, La, Ba, and Eu in each model. Chemical enrichment in forming ω Cen is due to gas ejected from SNe II, AGB stars, and NSM: ejecta from SNe Ia is not considered, because chemical enrichment by SNe Ia ends up with a significant decrease of $[\alpha/\text{Fe}]$, which is not observed in JP10. In order to model chemical evolution of ω Cen, we adopt chemical yields from Kobayashi et al. (2006, K06) for SNe II, Fishlock et al. (2014; F14) for AGB stars, and Tsujimoto & Shigeyama (2014) for NSMs. Chemical yield tables appropriate for low-metallicity stars are chosen from these theoretical predictions by K06 and F14. It should be noted here that chemical yields used in B17b are different from F14 adopted in the present study.

2.6.1. SNe II

Since chemical enrichment processes by SNe II are described by B17b in detail too, we briefly summarize them here. Gaseous ejecta from a SNe II can mix with its surrounding SPH particles so that the gas particles can increase their chemical abundances. Each SN can eject SPH gas particle with an initial ejection speed of v_{ej} , which is estimated from the following equation:

$$f_{\text{kin}} E_{\text{sn}} = 0.5(m_{\text{s}} - m_{\text{rem}})v_{\text{ej}}^2, \quad (6)$$

where f_{kin} , which is set to be 1, is the fraction of kinetic energy in total SN energy and m_{rem} is the mass of a neutron star or a black hole that is left after SN explosion for massive stars. Neutron stars that are left after SNe II can be the source of Eu in the present study (if they are pairs of neutron stars). For $m_{\text{s}} = 8M_{\odot}$ and $f_{\text{kin}} = 1$, $v_{\text{ej}} = 3800 \text{ km s}^{-1}$ ($m_{\text{ej}} = 6.5M_{\odot}$) and we adopt these values for all SNe II. The kinetic energy of a SN is distributed equally among SPH gas particles surrounding the SN.

2.6.2. SNe Ia

We consider that chemical enrichment by SNe Ia should not proceed in the early formation phase of ω Cen owing to no/little evolution of $[\alpha/\text{Fe}]$ with $[\text{Fe}/\text{H}]$ (JP10). Accordingly, chemical enrichment by SNe Ia is not included in all models of the present study. This assumption of no SNe Ia over the period of $\sim 300 \text{ Myr}$ in GC formation would not be so rea-

Table 1. References for previous works that suggested long (> 1 Gyr) and short (< 1 Gyr) formation timescale of ω Cen. See Stanford et al. (2006) for a detailed discussion on the methods to derive ages of stellar populations of ω Cen in these works.

Long timescale	Norris & Da Costa (1995), Hilker & Richtler (2000), Hughes & Wallerstein (2000), Smith et al. (2000), Lee et al. (2002), Origlia et al. (2003), Sollima et al. (2005), Stanford et al. (2006), Villanova et al. (2007)
Short timescale	Pancino et al. (2002), Ferraro et al. (2004), D’Antona et al. (2011), D’Orazi et al. (2011), this work

Table 2. The adopted $[\text{La}/\text{Fe}]$ for different stellar masses predicted from previous works (F14). Four different models for the yields are investigated for comparison and the yields for Y1 model are exactly the same as those in F14. The La yields for Y2, Y3, and Y4 are increased by 0.2, 0.25, and 0.3 dex, respectively, with respect to Y1. The Ba yields in Y2, Y3, and Y4 are also increased in the same way as La accordingly.

Model ID	$4M_{\odot}$	$5M_{\odot}$	$6M_{\odot}$	$7M_{\odot}$
Y1	0.72	0.64	0.52	0.20
Y2	0.92	0.84	0.72	0.40
Y3	0.97	0.89	0.77	0.45
Y4	1.02	0.94	0.82	0.50

sonable, if SNe Ia can occur only $\sim 10^8$ yr after star formation (“prompt SNe Ia”). However, it is observationally difficult to constrain the minimum delay time of SNe Ia (i.e., time lag between the formation of a binary pair of stars and the onset of SNe Ia explosion from the binary merging) through a comparison between chemical evolution models and observations (e.g., see Figure 9 in Siegel et al. 2019). Therefore, the assumption of no SNe Ia within a few Myr is not unreasonable in the present study. It would be possible that all ICM can be removed by other physical processes (such as ram pressure stripping) ~ 300 Myr after star formation in ω Cen. If this is the case, SNe Ia ejecta cannot mix with ICM to form new stars: SNe Ia cannot contribute to the chemical evolution of ω Cen. We will discuss this point later in §4.

2.6.3. AGB

Each AGB star is assumed to eject gas with a wind velocity of ~ 10 km s $^{-1}$ and the chemical abundances consistent with the adopted chemical yield table (F14). In order to model star formation directly from AGB ejecta without being diluted by gas, we adopt the following “AGB particle” model (Bekki 2019b; B19b). In the AGB particle model, soon after a new star enters into its AGB phase, a new SPH gas particle (“AGB particle”) is ejected from the star with its initial speed (v_w) of 10 km s $^{-1}$ with respect to the star. Accordingly, if this new gas particle is converted into a new star, then the new star can have chemical abundances that are the same as the AGB ejecta from which the gas originates. In previous galaxy-scale simulations (B13, B15), AGB ejecta is mixed with neighboring gas particles so that the ejecta can be diluted by ISM to have chemical abundances similar to those of ISM. The new AGB particle method can avoid this dilution that does not always occur in ICM. The new AGB particle can be mixed with SNe II and NSM ejecta if it is close to SNe II and NSM events.

There is a significant uncertainty in the predicted AGB yields for [Ba/Fe] and [La/Fe] over $-1.7 < [\text{Fe}/\text{H}] < -0.3$ (e.g., Busso et al. 2001; see also Figure 1 in Tsujimoto & Bekki 2012, which shows ~ 2 orders of magnitudes difference in the predicted yields for $-2 < [\text{Fe}/\text{H}] < -1$). Furthermore, the low yields for La predicted in F14 (e.g., [Ba/Fe] ~ 0.4 and [La/Fe] ~ 0.2 for $m = 7M_\odot$) cannot simply explain the observed significant fraction of stars with [La/Fe] ~ 0.5 in ω Cen (e.g., JP10). We therefore investigate different sets of models in which [Ba/Fe] and [La/Fe] are different by a factor of 3 in order to find the best set of models that can reproduce the observed range of [Ba/Fe] and [La/Fe]. We mainly shows the models in which Ba and La yield are by a factor of 2 larger than those shown in F14, because the models show that [Ba/Fe] and [La/Fe] at higher metallicities (> -1) are

more consistent with observations. The four yield models for AGB stars used in the present study (Y1, Y2, Y3, and Y4 with Y1 being exactly the same as F14) are briefly summarized in Table 2. We also compare between the results from different models.

AGB stars from 2G population can also chemically enrich ICM in the later phase of ω Cen formation, though such enrichment processes are much less significant than those by 1G AGB stars. However, it is possible that the time evolution of s -process elements with $[\text{Fe}/\text{H}]$ can be significantly influenced by the 2G AGB stars, because $[\text{Ba}/\text{Fe}]$ and $[\text{La}/\text{Fe}]$ of AGB ejecta depends strongly on $[\text{Fe}/\text{H}]$ (see Figure 1 in Tsujimoto & Bekki 2012, TB12). We therefore incorporate such chemical enrichment processes into some models based on the following relation (TB12) for $[\text{Fe}/\text{H}] < -1$:

$$[\text{Ba}/\text{Fe}] = [\text{Ba}/\text{Fe}]_0 + 0.6([\text{Fe}/\text{H}] - [\text{Fe}/\text{H}]_0), \quad (7)$$

where $[\text{Ba}/\text{Fe}]_0$ is $[\text{Ba}/\text{Fe}]$ at $[\text{Fe}/\text{H}]_0 = -1.7$. Once a 2G star enters into the AGB phase, the neighboring gas particles are assumed to be chemically polluted by the AGB wind. The Ba and La yields are calculated from (i) F14 and (ii) the above equation for $[\text{Fe}/\text{H}]$ of the star, and the chemical abundances of the gas particles are changed accordingly. Although we investigated how the existing field AGB stars of ω Cen’s host dwarf galaxy influence the chemical evolution of s -process elements, we found that such chemical enrichment processes by the field stars do not change the present results as long as the mass ratio of the field stars to the original GMC (m_2) is less than 3. Therefore, we do not show these results in the present study.

2.6.4. NSM

The details of mixing processes of NSM in forming GCs are yet to be fully understood, because no hydrodynamical simulations on this have ever been done. All of the NSM ejecta is assumed to be mixed well with and consequently retained in ISM of galaxies in our recent study of galactic chemical evolution (e.g., Tsujimoto et al. 2017). The assumed 100% retention of NSM ejecta in ISM would not be so realistic for ICM, because the total gas mass of ICM is much smaller than ISM of galaxies (BT17). Accordingly, we here adopt two different mixing models: (i) density-dependent and (ii) uniform mixing models. The density-dependent model is described as follows. BT17 showed that gaseous ejecta from NSM can be trapped by ICM within a GC, only if the density of ICM (ρ_{icm}) is rather high ($> 10^4$ atom cm^{-3}). In order to model this retention of NSM ejecta by ICM, we use the following formula for the stopping length (l_s) of NSM ejecta:

$$l_s = l_{s,0} \left(\frac{\rho_{\text{icm}}}{\rho_{\text{icm},0}} \right)^{-1} \text{pc}, \quad (8)$$

where $\rho_{\text{icm},0}$ is the reference density of the ICM that is set to be $10^5 \text{ atom cm}^{-3}$ (BT17) and $l_{\text{s},0}$ is the stopping length for $\rho_{\text{icm},0}$. In this formula, high-speed NSM ejecta can be retained by ICM only after it travels l_{s} . In the present study, we investigate the models with $l_{\text{s},0} = 0.27 \text{ pc}$, 0.78 pc , and 2.3 pc .

The neighboring gas particles around one NSM event are first searched within $r \leq r_{\text{nsm}}$ of the NSM, where r_{nsm} is the mixing length of NSM ejecta. Since the distance between a NS merger and one of its (j th) neighboring gas particles (r_j) can be larger than l_{s} , only a fraction of the total mass of the NSM ejecta can be retained by ICM. The total mass of NSM ejecta retained by j th gas particle ($m_{\text{nsm},j}$) is described as follows:

$$m_{\text{nsm},j} = f_{\text{ret}} \frac{m_{\text{nsm}}}{N_{\text{nei}}}, \quad (9)$$

where m_{nsm} is the total mass of NSM ejecta, f_{ret} is the mass fraction of NSM ejecta retained by the gas particle, and N_{nei} is the total number of neighboring gas particles around the NS merger. Here it is assumed that NSM ejecta can be distributed among all of its neighboring gas particles. In order to estimate f_{ret} , we consider that the gas particle has a spherical shape with a radius h_j , where h_j is the SPH smoothing length, and (ii) the flux per unit area for NSM ejecta at the position of the gas particle is as follows:

$$F_{\text{nsm},j} = \frac{m_{\text{nsm}}}{4\pi r_j^2}. \quad (10)$$

Accordingly, f_{ret} is as follows:

$$f_{\text{ret}} = \pi h_j^2 F_{\text{nsm},j}. \quad (11)$$

If r_j is much smaller than h_j , f_{ret} can be larger than 1 in the above formula. For that case, f_{ret} is set to be 1.

The uniform mixing model is as follows. All gas particles around each NSM event can be uniformly polluted by NSM in this model, even if the physical properties of the gas particles are quite different. Accordingly, f_{ret} is a free parameter ranging from 0 to 1 and needs to be chosen such that the observed $[\text{Eu}/\text{Fe}]$ of ω Cen can be reproduced. Since l_{s} is not introduced in this model, the mixing radius (r_{nsm}) is also a free parameter. We investigate the models with $r_{\text{nsm}} = \epsilon_{\text{g}}$, and $10\epsilon_{\text{g}}$, where ϵ_{g} is the gravitational softening length of gas particles. We mainly show the results of the density-dependent models for mixing of NSM ejecta, because they are more realistic.

In order to calculate the number of NSM events per unit stellar mass for a given IMF, we assume that the ratio of NSM events per one SNe II (r_{nsm}) is 10^{-3} . We however investigate models with different r_{nsm} in the present study. The delay time distribution (DTD) of NSM ($N_{\text{nsm}}(t)$) is as follows:

$$N_{\text{nsm}}(t) = N_{\text{nsm},0} (t/t_{\text{nsm}})^{-1}, \quad (12)$$

where $N_{\text{nsm},0}$ is the normalization factor and t_{nsm} is a parameter that determines the DTD (e.g., Dominik et al. 2012). For most models, we assumed that NSM occurs between 10^7 yr to 10^{10} yr and t_{nsm} is set to be 10^7 yr. We also investigate the models with a different $N_{\text{nsm}}(t)$ just for comparison. We consider that (i) $0.01M_{\odot}$ can be ejected from one NSM event, (ii) the mass fraction of Eu in the ejecta (f_{eu}) is 0.01, and (iii) [La/Eu] and [Ba/Eu] are set to be -0.2 and -0.1 , respectively, which are reasonable for stars with $[\text{Fe}/\text{H}] \sim -1.7$ ω Cen (e.g., Fig. 4 in D11). If we consider NSM ejecta consisting of elements with mass numbers larger than 90, then $f_{\text{eu}} = 4.8 \times 10^{-3}$ rather than 0.01. This factor of ~ 2 difference in Eu yield does not change the present results so much.

2.7. Parameter study

We mainly describe the results for the fiducial model with $M_{\text{gmc}} = 2 \times 10^7 M_{\odot}$, $R_{\text{gmc}} = 140$ pc, $r_{\text{gmc}} = 0$ kpc (i.e., located in the center of its host dwarf), firstly because the final stellar mass of the simulated GC can be as large as $\sim 10^7 M_{\odot}$ that is 2 – 3 times larger than the present-day mass ($\sim 4 \times 10^6 M_{\odot}$), and secondly because the total mass of He-rich stars can be as large as $[6 - 8] \times 10^5 M_{\odot}$ as observed (e.g., Norris 2004). The initial total number of particles (N) is set to be 1040000 in the fiducial model, and N increases significantly owing to the ejection of new AGB particles from AGB stars during a simulation. The mass and size resolutions are $10M_{\odot}$ and 2 pc, respectively, in the fiducial model. The values of basic parameters adopted in the fiducial model are given in Table 3.

We investigate how the total masses, sizes, and initial locations of GMCs determine the final physical properties of GCs by changing the basic parameters, M_{gmc} , R_{gmc} , and r_{gmc} . We also investigate how the present results depend on the model parameters for mixing processes of NSM ejecta (e.g., uniform or density dependent mixing) in order to make robust conclusion on the results. In the present study, [Ba/Fe]–[Fe/H], [La/Fe]–[Fe/H], and [Eu/Fe]–[Fe/H] relations depend strongly on the details of the modeling for NSM ejecta mixing. We therefore extensively investigate how these relations can be controlled by model parameters for NSM ejecta mixing. We show the results of only 22 representative models, though we have investigated 30+ models. The parameter values of these representative models with are summarized in Table 4. In the followings, 1G and 2G stars means (i) new stars formed from original gas particles and those formed from gas ejected from AGB stars, whenever they are formed. Accordingly, new stars formed from re-accreted original gas after 2G star formation has started are also identified as “1G”, though they can be younger than some of the 2G stars formed earlier.

Table 3. Description of the parameter values for the fiducial model. One of key elements in the model is that new gas particles are ejected from one AGB star (“AGB particle” method) to allow the AGB ejecta to be converted into new stars without dilution.

GMC mass	$M_{\text{gmc}} = 2 \times 10^7 M_{\odot}$
GMC radius	$R_{\text{gmc}} = 140 \text{ pc}$
GMC scale radius	$R_{\text{gmc}} = 27 \text{ pc}$
GMC initial position	$r_{\text{gmc}} = 0 \text{ pc}$
Initial virial ratio	$t_{\text{vir}} = 0.4$
Fraction of rotational energy	$f_{\text{rot}} = 0.01$
Fractal dimension	$D_3 = 2$
Mixing of NSM ejecta	Density-dependent ($r_{\text{nsm}} = 0.55 \text{ pc}$)
Threshold density for star formation	$\rho_{\text{th}} = 10^5 \text{ atom cm}^{-3}$
Simulation code	B17b
Mass resolution	$19 M_{\odot}$
Size resolution	0.55 pc
AGB yield	F14
SNe II yield	K06
NSM yield	TS14
SNe II feedback effects	Included
SNe Ia feedback effects	Not included
AGB feedback effects	Included
AGB wind velocity	10 km s^{-1}
AGB particle method	Included

3. Results

3.1. The fiducial model

3.1.1. Spatial distributions and kinematics of He-poor and He-rich stars

Figure 1 shows how the projected distributions of “He-poor” ($Y \leq 0.25$) and “He-rich” ($Y > 0.25$) stars at $T = 300$ Myr are different in the simulated ω Cen for the fiducial model M1. Clearly, both He-poor and He-rich populations shows rather flattened shapes in all three projections with the major axes of the shapes of the two populations being aligned with each other. The He-rich population shows a stronger central mass concentration, which reflects that it is formed from gas that is ejected from AGB stars and then accumulated into the deeper potential well of the forming GC. Although the simulated flattened distributions are qualitatively consistent with the observed shape of ω Cen, it should be noted here that the present simulations does not investigate long-term two-body relaxation processes that significantly changes the shapes of GCs (e.g., Mastrobuono-Battisti & Peters 2016). It could be possible that the simulated GC can become significantly less flattened owing to such dynamical effects, though the two body relaxation timescale is longer for ω Cen.

Figure 2 demonstrates that the He-poor population has a small amount of rotation ($V_{\max} \sim 2 \text{ km s}^{-1}$, where V_{\max} is the maximum rotational speed) within the central 30 pc in the three 2D kinematic maps. This global rotation of the He-poor population inherits from the initial angular momentum of its natal GMC with $f_{\text{rot}} = 0.01$. Accordingly, the final amplitude of the rotation in the He-poor population of the simulated ω Cen depends strongly on f_{rot} in the present study. The He-rich population, on the other hand, does not show clear rotation in the three 2D kinematic maps. This result is in a striking contrast with our previous works (Bekki 2011), which demonstrates that 2G stars formed from 1G AGB ejecta in a GC (corresponding to the He-rich population in the present study) can have a significant amplitude of rotation within the GC.

Significant differences between the present study and our previous ones are as follows. First, the present study simulates GC formation from initial star formation from natal GMCs (i.e., 1G formation) of GCs whereas previous ones investigated star formation from AGB ejecta in existing (1G) stellar systems. Second, the feedback effects of SNe II from 2G stars are included in the present study, but not in previous ones. Third, all AGB ejecta is assumed to be similarly rotating with respect to the center of the existing stellar system in previous works, whereas such initial uniform rotation is not assumed in the present study: the initial angular momentum of AGB ejecta can be quite different between different AGB stars. The second difference is the main physical reason for the less amount of rotation in the He-rich

stars in the fiducial model. SNe II feedback effects can stir the ICM so that the new stars formed from the ICM cannot have a large degree of ordered motion in the present study.

3.1.2. Abundance distribution functions (ADFs)

Figure 3 describes the abundance distribution functions (ADFs) of the 11 elements investigated in the fiducial model. The strong peak in each abundance corresponds to the abundance of 1G population and thus to that of its natal GMC. Unlike the observed ADF of $[\text{Fe}/\text{H}]$ in ω Cen, the simulated ADF does not show clearly distinct multiple peaks around $[\text{Fe}/\text{H}] \sim -1.4$ (corresponding to “RGB-Int1”; see Figure 8 in JP10), ~ -1.1 (“RGB-Int2+3”), and 0.6 (“RGB-a”). Also, the observed ADF shows a broad peak around $[\text{Fe}/\text{H}] \sim -1.7$ (“RGB-MP”), which is not *assumed* in the present model: the simulated very sharp peak around $[\text{Fe}/\text{H}] \sim -1.7$ is due simply to the adopted assumption of a single metallicity in the GMC. If a GC-forming GMC is initially very massive, as assumed for ω Cen in the present work, the GMC can possibly have a significant metallicity spread, which can end up with a broad peak of the ADF for 1G stars formed within the GMC.

The ADF of Y in this model shows three peaks around $[\text{Fe}/\text{H}] \approx 0.25$, ≈ 0.31 , and ≈ 0.36 . In the adopted chemical yields for AGB stars (F14), massive AGB stars can eject gas with higher Y (~ 0.36). Therefore, the third peak around $Y \sim 0.36$ corresponds to the secondary star formation from gas ejected from massive AGB stars ($m > 6M_{\odot}$). The second peak in the ADF of Y (~ 0.31) is due to the formation of new stars from gas ejected from less massive AGB stars. As shown in Figure 4, the third peak of Y is the most pronounced for stars with $-1.6 < [\text{Fe}/\text{H}] \leq -1.3$, which means that a larger fraction of new stars with high Y can be formed AGB ejecta that is not so much polluted by SNe II ejecta. Clearly, there are stars with normal Y (~ 0.25) yet higher $[\text{Fe}/\text{H}]$ (> -1.6) in Figure 4, though the number fraction of such stars is quite small. These He-poor and Fe-rich stars are formed from pristine gas that is later accreted onto the existing stellar system, partially polluted by SNe II ejecta, and finally converted into new stars in the central region of the system.

Figure 3 demonstrates that the simulated ADF is bimodal for $[\text{C}/\text{Fe}]$, $[\text{N}/\text{Fe}]$, $[\text{O}/\text{Fe}]$, and $[\text{Na}/\text{Fe}]$. The physical origin of these bimodal ADFs is caused by the efficient formation of 2G new stars almost directly from AGB ejecta with low $[\text{O}/\text{Fe}]$ and high $[\text{C}/\text{Fe}]$, $[\text{N}/\text{Fe}]$, and $[\text{Na}/\text{Fe}]$. In this model, no dilution of AGB ejecta by pristine (original) gas can occur so that the chemical abundance patterns of some 2G stars can be almost exactly the same as those of AGB ejecta. This no/little dilution of AGB ejecta is one of characteristics of ω Cen’s chemical evolution: it should be noted here that dilution of AGB ejecta by pristine gas is essential for explaining chemical abundance patterns of other “ordinary” GCs with

multiple stellar populations (e.g., B07). As shown in Figure 4, the locations the peaks in the $[O/Fe]$ distribution is significantly different for the two $[Fe/H]$ ranges, i.e., $[Fe/H] \leq -1.6$ and $-1.6 < [Fe/H] \leq -1.3$. However, the peak locations of the distributions in the three ranges for $-1.6 < [Fe/H]$ are not so different. These $[Fe/H]$ -dependent ADFs can be seen for $[Na/Fe]$ in Figure 4, though the ADF of $[Na/Fe]$ for higher $[Fe/H]$ is significantly wider than that of $[O/Fe]$. It should be stressed that there are stars with rather high $[Na/Fe]$ (> 1) only for the highest $[Fe/H]$ range (> -0.5), though the number fraction is quite small. These high- $[Na/Fe]$ stars can be formed from gas polluted by SNe II whose progenitor stars have higher metallicities in the chemical yield table by K06.

As shown in Figure 3, the ADFs of $[Mg/Fe]$ and $[Al/Fe]$ are not bimodal and they are not so broadened by the formation of 2G stars from AGB ejecta. This is mainly because $[Mg/Fe]$ and $[Al/Fe]$ in the adopted AGB yields (for 2G stars) are not so much different from those adopted for the initial GMC. The ADFs of the two s -process elements, $[Ba/Fe]$ and $[La/Fe]$, have a strong peak around the initial abundances with a very wide “skirt” ranging from -1 to 1 . Since Ba and La can be produced both by AGB stars and NSM at different epochs, their ADFs can be significantly broadened after the formation of 2G stars from AGB ejecta mixed with NSM one. The ADF of $[Ba/Fe]$ for $[Ba/Fe] > 0$ has a broad peak around $[Ba/Fe] \approx 0.7 - 1$ in this model.

As shown in Figure 4, the location(s) of the peak(s) and the level of broadening in the ADF of $[La/Fe]$ are quite different between different $[Fe/H]$ ranges. These simulated ADFs of $[La/Fe]$ for different metallicity ranges are not so consistent with the observed ones by JP10 (see Figure 12 of JP10). For example, the observed ADF does not show its peak at $[La/Fe] < 0$, and there is no stars with $[La/Fe] < 0$ for $[Fe/H] > -0.9$ (JP10). The simulated ω Cen, however, has a large fraction of stars with $[La/Fe] < 0$ for $[Fe/H] > -0.9$ and the peak around $[La/Fe] \sim 0.1$ for $[Fe/H] > -0.9$. Such a large fraction of stars with low $[La/Fe]$ is due to star formation from gas polluted too much by SNe II, because SNe II ejecta can lower $[La/Fe]$ of ICM. The observed ADF of $[La/Fe]$ has only one peak for $-1.6 < [Fe/H] < -1.3$ and for $-1.3 < [Fe/H] < -0.9$ whereas the simulated one show two peak for the two $[Fe/H]$ ranges. These results that are not so consistent with observations suggest that the present chemodynamical study misses key physical processes in the mixing of AGB and SNe II ejecta.

Observations showed that $[Eu/Fe]$ ranges from ~ -0.5 to ~ 0.8 in ω Cen (Figure 17 of JP10), which is a significantly wider distribution compared to the Galactic halo stars with metallicities similar to ω Cen. There are a fraction of stars that have negative $[Eu/Fe]$ in ω Cen, though there are no such stars in the Galactic halo with the same metallicity range as ω Cen (Figure 17 of JP10). Such stars with negative $[Eu/Fe]$ for $[Fe/H] > -1.7$ are indeed formed in the fiducial model, as shown in Figure 3. The physical reason for this is as follows.

Although NSMs can increase $[\text{Eu}/\text{Fe}]$ of ICM and thus $[\text{Eu}/\text{Fe}]$ of new stars, such an increase cannot be so dramatic due to the retention capability of NSM ejecta by ICM. First of all, the total mass of ICM during 2G formation cannot be as large as $\sim 10^6 M_\odot$ that is required for the full mixing of NSM ejecta in ISM of galaxies (Tsujiimoto et al. 2017), firstly because the total mass of AGB ejecta (i.e., the dominant component of ICM) can be at most 5% of 1G stars, secondly because the AGB ejecta continues to be consumed by star formation. Also, the mass density of ICM around some NSM events can be quite low so that NSM ejecta cannot be retained so well: rather high mass-density is required for efficient retention of NSM ejecta in this model with the density-dependent mixing model. Thus, NSM ejecta can be only partially retained in ICM of forming ω Cen in this model.

Owing to the partial retention of NSM ejecta, $[\text{Eu}/\text{Fe}]$ decrease of ICM due to chemical enrichment by SNe II can be more significant than $[\text{Eu}/\text{Fe}]$ increase by NSMs in some local regions of ICM. Accordingly, new stars formed from such local regions can have negative $[\text{Eu}/\text{Fe}]$: those formed from local regions where SNe II chemical enrichment is much less efficient can still have positive $[\text{Eu}/\text{Fe}]$. Therefore, $[\text{Eu}/\text{Fe}]$ of a 2G star depends on whether the natal gas of the star is polluted by NSM or SNe II to a greater extent. If all NSM ejecta can be retained in ICM, then $[\text{Eu}/\text{Fe}]$ can be as large as ~ 2 , as shown later. The observed lack of such stars with large $[\text{Eu}/\text{Fe}]$ in ω Cen means that only a small portion of NSM ejecta could be retained by ICM in the early formation phase of ω Cen. Stars with low $[\text{Eu}/\text{Fe}]$ (< 0) at $[\text{Fe}/\text{H}] > -1.7$ observed in ω Cen do not exist in the Galactic stellar halo (JP10), which implies that the chemical enrichment process of r -process elements can be quite different between ω Cen and the building blocks of the Galactic stellar halo.

3.1.3. Radial abundance gradients

As shown in Figure 5, the simulated ω Cen has a negative radial gradient of Y within the central 10pc, which is also consistent with the more compact distribution of He-rich stars in Figure 1. This strong concentration of 2G stars with high Y (and low $[\text{O}/\text{Fe}]$) is also consistent with observations by Sollima et al. (2007) and Gratton et al. (2011). The main reason for this negative gradient is that He-rich stars from AGB ejecta can be formed mostly in the central region of this GC where the low velocity AGB wind can be captured efficiently. The 1σ dispersion in Y at each radial bin is quite large (~ 0.05), which is due largely to the co-existence of stars with rather high Y (~ 0.34) and normal Y (~ 0.25) in the central 10pc.

In order to compare these results with corresponding observations, we here use the observed number ratio (f_{bms}) of blue main-sequence (bMS) to red main-sequence stars (rMS)

in ω Cen (Sollima et al. 2007). The number ratio as a function of R (distance from ω Cen’s center in units of arcmin) is described as follows:

$$f_{\text{bms}} = 0.16 - 0.027(R - 12). \quad (13)$$

By assuming that Y is 0.25 for rMS and 0.35 for bMS, we can convert this relation into a radial dependence of Y . The blue dotted line in Figure 5 describes the negative slope of Y observed in ω Cen, though the observed f_{bms} shows an apparently sharp decline with increasing R . Only 0.01 change in Y over 10 pc in the observed Y gradient of ω Cen is significantly shallower than the simulated one. The simulated steeper Y gradient at the birth of ω Cen might not be a serious problem, because the long-term dynamical evolution can make the gradient shallower.

Clearly, the simulated GC shows a negative radial gradient of $[\text{Fe}/\text{H}]$ too, which is not so consistent with the observed apparently flat gradient in JP10, however. The simulated $[\text{Fe}/\text{H}]$ gradient means that a significant fraction of new stars can be formed from AGB ejecta in the central region of ω Cen after the ejecta is mixed well with SNe II ejecta. The large 1σ dispersion in each $[\text{Fe}/\text{H}]$ radial bin is caused by the co-existence of stars formed from ICM with different $[\text{Fe}/\text{H}]$ at different epochs. Since population mixing due to the long-term dynamical evolution of the cluster caused by two-body relaxation effects can possibly smooth out the original radial gradient of $[\text{Fe}/\text{H}]$, the radial gradient can possibly become flatter as observed. However, we need to investigate this point in our future work.

Although the radial gradients of $[\text{N}/\text{Fe}]$ and $[\text{C}/\text{Fe}]$ are weak and negative (~ -0.06 dex pc^{-1}) in the simulated ω Cen, the radial $[\text{O}/\text{Fe}]$ gradient is positive (~ 0.02 dex pc^{-1}). The lower $[\text{O}/\text{Fe}]$ in the inner region is due to the presence of 2G stars that are formed from gaseous ejecta with rather low $[\text{O}/\text{Fe}]$ from massive AGB stars. The larger $[\text{C}/\text{Fe}]$ in the central region is due to the higher fraction of carbon-rich stars: stars with $[\text{C}/\text{Fe}]$ dominates in the $[\text{C}/\text{Fe}]$ distribution for $[\text{Fe}/\text{H}] > -1.6$ in Figure 3. The slope of the radial gradient of $[\text{Na}/\text{Fe}]$ is weakly positive with a large 1σ dispersion (~ 0.3 dex) in each radial bin. The radial gradients of $[\text{Mg}/\text{Fe}]$ and $[\text{Al}/\text{Fe}]$ are rather flat with small dispersions. Since JP10 did not show the radial gradient of $[\text{Mg}/\text{Fe}]$, it is currently not possible for the present study to discuss the consistency of the results with observations.

There are very weak negative radial gradients for $[\text{La}/\text{Fe}]$ and $[\text{Ba}/\text{Fe}]$ (~ -0.02 dex pc^{-1}) with 1σ dispersions larger in the inner regions. The radial profile of $[\text{Eu}/\text{Fe}]$ shows a weakly positive slope, which is caused by a larger fraction of 2G stars with low $[\text{Eu}/\text{Fe}]$ that are formed from ICM polluted heavily by SNe II. The radial profiles of $[\text{Fe}/\text{H}]$, $[\text{O}/\text{Fe}]$, $[\text{Na}/\text{Fe}]$, $[\text{Al}/\text{Fe}]$, $[\text{La}/\text{Fe}]$, and $[\text{Eu}/\text{Fe}]$ for ω Cen are shown in Figure 9 of JP10, though the amplitudes of the slopes of the radial gradients are not described.

3.1.4. Relations between Y , $[X/Fe]$, and $[Fe/H]$

As shown in Figure 6, Y and $[X/Fe]$ depend strongly of $[Fe/H]$ only for a narrow range of $[Fe/H]$ ($-1.7 < [Fe/H] < -1.5$). Y , $[C/Fe]$, $[N/Fe]$, $[Na/Fe]$, $[Mg/Fe]$, $[Al/Fe]$, $[Ba/Fe]$, and $[La/Fe]$ increase with increasing $[Fe/H]$ whereas $[O/Fe]$ and $[Eu/Fe]$ decrease with increasing $[Fe/H]$. The derived rapid increase/decrease of these abundances are due largely to 2G formation from AGB ejecta mixed with SNe II ejecta, as explained for other figures. The simulated $Y-[Fe/H]$ relation and $[X/Fe]$ relations for C, N, O, Na, Mg, Al are almost flat for $[Fe/H] > -1.5$: $[C/Fe]$ and $[N/Fe]$ very slightly decrease with increasing $[Fe/H]$. Since $[C/Fe]$ of SNe II ejecta ranges from -0.18 to -0.4 in the adopted yields (K06), new stars formed from ICM mixed with SNe II ejecta can show lower $[C/Fe]$. Therefore, the decrease of $[C/Fe]$ at $[Fe/H] > -1.5$ is due to the enrichment of ICM by SNe II. $[Ba/Fe]$ and $[La/Fe]$ clearly decrease with increasing $[Fe/H]$ for $[Fe/H] > -1.3$. Although the steady increase of $[Ba/Fe]$ and $[La/Fe]$ with increasing $[Fe/H]$ for $[Fe/H] < -1.5$ in the simulated ω Cen is indeed seen in observations (Figure 10 of JP10), though $[\alpha/Fe]-[Fe/H]$ relations for the two are observed to be flat for $[Fe/H] > -1.5$ in JP10. Observational studies of ω Cen by D11, however, shows a slight decrease of $[La/Fe]$ with increasing $[Fe/H]$ after its peak around $[Fe/H] \approx -1$.

The simulated $[Eu/Fe]-[Fe/H]$ relation shows a steady decrease with increasing $[Fe/H]$, which is not so consistent with the observed relation with an almost constant $[Eu/Fe]$ over a wide range of $[Fe/H]$ (JP10). It should be stressed here that the evolution of $[Eu/Fe]$ with $[Fe/H]$ is not so clear for $[Fe/H] > -1.0$ owing to a very small number of data points beyond $[Fe/H] > -1.0$ in JP1: it should be noted here that D11 shows a decreasing $[Eu/Fe]$ with increasing $[Fe/H]$. The main physical reason for the steady decrease of $[Eu/Fe]$ with increasing $[Fe/H]$ is as follows. Although NSM ejecta can be mixed with high-density ICM polluted by AGB ejecta, a large fraction of the ejecta can be expelled from the ICM in this model so that $[Eu/H]$ can only slowly increase. Accordingly, SNe II ejecta, which dramatically increases $[Fe/H]$ of ICM if it is trapped by ICM, can decrease $[Eu/Fe]$ of ICM rather quickly after its mixing with ICM. Thus new stars formed from ICM that is chemically polluted by SNe II to a much larger extent than by NSM can have rather low $[Eu/Fe]$. The amount of AGB ejecta that can trap NSM ejecta ($< 10^6 M_\odot$) is so small in this forming ω Cen that chemical enrichment by SNe II can proceed more rapidly than that by NSMs. A way to reproduce the observed $[Eu/Fe]-[Fe/H]$ relation better is discussed in the next subsection on the parameter dependence.

3.1.5. Relations between ages and chemical abundances

Figure 7 describes the relations between ages and chemical abundances (e.g., Y and $[\text{Fe}/\text{H}]$) estimated over ~ 300 Myr for 11 elements in the simulated ω Cen. Here the “age” of a star in a simulation is the difference between the formation epoch of the star and the final time of the simulation: “zero age” means the youngest star in the simulation and the oldest star is 300 Myr old. The key results of Figure 7 are as follows. First, the age metallicity relation (AMR: age- $[\text{Fe}/\text{H}]$ relation) is steep only for stars with ages older than 200 Myr, and the AMR is quite flat for those younger than 200 Myr. Although stars with higher metallicities ($[\text{Fe}/\text{H}] \sim -0.5$) can be formed from ICM heavily polluted by SNe II of 2G stars in the later stage of ω Cen formation in this model, new stars with lower $[\text{Fe}/\text{H}]$ can be also formed from AGB ejecta not so heavily polluted by SNe II. As a result of this, the mean $[\text{Fe}/\text{H}]$ for younger stars cannot be so high.

Second, steep relations between ages and chemical abundances can be seen for Y , $[\text{C}/\text{Fe}]$, $[\text{N}/\text{Fe}]$, and $[\text{O}/\text{Fe}]$ for ages older than 240 Myr, which is due to the 2G formation from AGB ejecta. These age-abundance relations are rather flat for stars younger than 240 Myr. Third, age-abundance relations are fairly flat for $[\text{Na}/\text{Fe}]$, $[\text{Mg}/\text{Fe}]$, and $[\text{Al}/\text{Fe}]$, though $[\text{Na}/\text{Fe}]$ depends weakly on ages for stars older than 160 Myr. Fourth, there is not a clear trend in the age-abundance relations in $[\text{Ba}/\text{Fe}]$ and $[\text{La}/\text{Fe}]$ for stars younger than 240 Myr, however, lower these abundances for younger ages can be seen for stars with ages older than 240 Myr. It should be stressed here that $[\text{La}/\text{Eu}]$ and $[\text{Ba}/\text{Eu}]$ for ages younger than 100 Myr are quite high (> 0.5 , i.e., dominated by s -process elements), which is consistent with observations by JP10, though they are negative for the oldest age bin. There is a flat age- $[\text{Eu}/\text{Fe}]$ relation for stars younger than 240 Myr, and $[\text{Eu}/\text{Fe}]$ is the highest in the oldest age bin corresponding to 1G stars.

3.1.6. Chromosome maps

Figure 8 describes the distributions of 1G and 2G stars on the $[\text{O}/\text{Na}]-[\text{Fe}/\text{H}]$ and $[\text{O}/\text{Fe}]-[\text{Fe}/\text{H}]$ maps, which can be compared with corresponding observations (e.g., Figure 18 in JP10). These maps are similar to “Chromosome map” shown in Figure 23 by Marino et al. 2019, which describes the observed distribution of stars on the $[\text{Na}/\text{Fe}]-[\text{O}/\text{Fe}]$ map. As shown in Figure 8, 1G and 2G stars are widely distributed on the $[\text{O}/\text{Fe}]-[\text{Fe}/\text{H}]$ map and there is a bimodal distribution for $[\text{Fe}/\text{H}] < -1.3$, which can be seen also in the observed map, though there is a large dispersion in the observed bimodal distribution. The simulated distribution shows a significant fraction of stars with $[\text{O}/\text{Fe}] > 0.5$ at $[\text{Fe}/\text{H}] > -1.3$, which is not observed. These stars with large $[\text{O}/\text{Fe}]$ (up to ~ 1.1) can be formed from ICM that are

polluted heavily by massive SNe II ($m > 30M_{\odot}$).

Since K06 assumes the broadly constant Fe yield, irrespective of the progenitor mass, [O/Fe] in the ejecta of massive SNe II is quite large. If other O and Fe yields from other papers (e.g., [O/Fe]=0.5 from Tominaga et al. 2007) are adopted, the fraction of such O-rich star can be reduced to the observed level. In order to demonstrate this point, a comparative model M1a with [O/Fe]=0.5 in massive SNe II is investigated, and the results are shown in Figure 8. Clearly, the level of consistency between the observed and simulated distributions of stars on this map is significantly higher in M1A than in M1. This result implies that it might be better for our future works on the chemical evolution of ω Cen to consider the Fe yields implied by the light curve analysis of supernovae, which indicates an increasing Fe yield with increasing progenitors mass (e.g., Tominaga et al. 2007).

1G and 2G stars are distributed on two narrow “stripes” on the [O/Fe]–[Fe/H] map for [Fe/H] < -1.3 whereas the observed bimodal distribution does not show a clear gap between the two groups ([O/Fe] ≈ -0.4 and ≈ 0.4). Since the natal GMC of ω Cen is assumed to have no [Fe/H] and [O/Fe] spreads, the 1G stars formed from the gas cannot show a wider distribution on the map. If such initial abundance spreads within a GMC is considered in future simulations, the observed distribution will be able to be better reproduced. Although the simulated distribution of stars on the [O/Na]–[Fe/H] map shows a bimodality for [Fe/H] < -1.3 , the overall distribution appears to be dissimilar to the observed one owing to the presence of stars with high [O/Na] (> 1) at [Fe/H] > -1.3 . The observed distribution appears to show two major groups of stars, one with [O/Na] ≈ -1 and the other with [O/Na] ≈ 0.4 , though there is no clear gap between the two groups. The group with lower [O/Na] in the simulated distribution has a bit too high [O/Na], which is again due to the adopted large [O/Fe] from massive SNe II. Intriguingly, the observed distribution has a very minor fraction (2 out of 29 stars; 6.9%) of stars with [O/Na] > 0 and [Fe/H] > -1 (“zone of avoidance”). This almost empty area on this map cannot be seen in the simulated distribution, which is an inconsistency between observations and the present simulation.

The origin of this apparent zone of avoidance is yet to be understood. First of all, it is not clear why this can be seen for a higher metallicity range ([Fe/H] > -1) only. Clearly a large fraction of stars at [Fe/H] < -1 shows high [O/Na] (> 0.5) in the observed ω Cen, which is consistent with new star formation from gas polluted by SNe II ejecta. The lack of such stars at [Fe/H] > -1 could be therefore due to a much smaller degree of chemical pollution of ICM by SNe II ejecta with high [O/Na] (high [O/Fe]) for that metallicity range. One possibility is that ICM is polluted only by low-mass SNe for [Fe/H] > -1 . It is beyond the scope of this paper, however, to discuss why [Fe/H] ≈ -1 is the “turning point” when the chemical enrichment processes by SNe II can significantly change: this should be one

of the key issues in our future studies. It should be noted here that the fraction of stars with $[O/Na] >$ and $[Fe/H] > -1$ is only 7.8%, which is only slightly (by 13%) higher than the observed value (6.9 %). Therefore, it could be possible that if $[O/Na]$ and $[Fe/H]$ are investigated for a much larger number of stars ($\approx 10^4$), then the above zone of avoidance disappears.

Figure 9 describes the distributions of 1G and 2G stars on the $[N/Fe]-Y$ map in the simulated ω Cen, which shows (i) one strong peak due to 1G stars and (ii) two elongated and wide distributions along $[N/Fe]$ -axis for $Y \sim 0.31$ and $Y \sim 0.35$. Clearly, He-rich stars can show a wide range of $[N/Fe]$ and are more likely to have higher $[N/Fe]$. The derived wide range of $[N/Fe]$ for a given Y is due to 2G formation from AGB ejecta with higher Y and higher $[N/Fe]$ that is mixed with SNe II ejecta with lower $[N/Fe]$ (< -0.8). Bellini et al. (2017) have recently revealed that although “bMS” stars (i.e., those on the blue main sequence on the CMD) have rather high Y and $[N/Fe]$, some stars (“MSd” population) have moderately high Y and moderately high $[N/Fe]$ (see their Table 1). These observed populations with different Y and $[N/Fe]$ are qualitatively consistent with the results in Figure 9. They have also identified 15 distinct subpopulations based on $[Fe/H]$, Y , and $[N/Fe]$ (see their Table 1), which are not clearly seen in Figure 9. The lack of multiple distinct peaks in Figure 9 reflect the fact that star formation is more continuous in the formation of 2G stars in the present study.

3.1.7. $[La/Eu]-[Fe/H]$ relation

One of the most intriguing observational results of ω Cen is that it shows a large $[La/Eu]$ (> 0.1) for $[Fe/H] > -1.2$ (e.g., S00, JP10, D11). Such a large $[La/Eu]$ cannot be seen in halo field stars of the Galaxy (JP10), which implies that the chemical evolution of ω Cen is quite different from that of the Galactic halo. Since this $[Eu/La]$ evolution depends strongly on the ejection rates of gas from AGB stars, NSMs, and SNe II, the observed trend with $[Fe/H]$ can be a strong constraint on the formation of ω Cen (JP10). As shown in Figure 10, $[Eu/Fe]$ rapidly increases with increasing $[Fe/H]$ and reaches its peak (~ 0.6) around $[Fe/H] = -1.5$. This rapid increase reflects the fact that AGB ejecta can be much more efficiently retained in ICM than NSM ejecta in ω Cen. Accordingly, these different degrees of retention capabilities of AGB and NSM ejecta in ω Cen formation can distinguish it from other GCs and halo field stars. The derived rapid increase is consistent with the observed trend by JP10, however, the location of the peak ($[Fe/H] \sim -1.5$) is a bit too metal-poor in comparison with the observed location ($[Fe/H] \sim -1$; D11). This apparent inconsistency implies that the chemical enrichment of the ICM by AGB stars in the simulated ω Cen can

proceed a bit too rapidly.

The simulated very slow decline of [La/Eu] with increasing [Fe/H] can be seen in the observed [La/Eu]–[Fe/H] relation (e.g., Figure 18 in JP10). Also, it should be stressed that observations show a minor fraction of stars with [La/Eu] < 0 for [Fe/H] > –1.2, which is also seen in the simulated ω Cen. The low and positive [La/Eu] (~ 0.2) at [Fe/H] ~ -0.5 in the simulated ω Cen is consistent with observations by JP10 and D11, which strongly suggests that this fiducial model can properly describe some key processes (but not all) in the mixing of AGB, NSM, and SNe II ejecta. Although observations do not clearly describe the dispersion of [La/Eu] for a given [Fe/H], the derived dispersions in this model appears to be compatible with the observed ones (JP10). It should be stressed that the adopted La yield is by a factor of 2.5 larger than that shown in F14. As discussed later, the models with lower La yields show low [La/Eu] (≤ 0) at [Fe/H] ~ -0.5 that is not consistent with observations.

3.2. Parameter dependence

It is confirmed that some properties of the simulated ω Cen depend strongly on the input parameters such as the degree of initial rotation of gas and the mixing process of AGB and NSM ejecta, though others do not. We here describes the key physical properties of ω Cen that depends strongly on model parameters in Figures 12–15.

3.2.1. Structure and kinematics of He-poor and He-rich populations

All of the present models with different parameters show a strong central concentration of He-rich stars in the simulated ω Cen: the 3D structure of He-rich stars do not depend on model parameters, M_{gmc} , R_{gmc} , and mixing processes of AGB and NSM ejecta. However, the projected 2D kinematics of He-poor and He-rich stars in the simulated ω Cen depend strongly on f_{rot} (i.e., the initial fraction of rotational energy in kinetic energy for the natal GMC). Figure 11 shows that the amplitudes of rotation for He-poor and He-rich populations are significantly enhanced in the model M2 with $f_{\text{rot}} = 0.03$. The maximum amplitude of rotation ($V_{\text{max}} \approx 5 \text{ km s}^{-1}$) in this M2 is more consistent with observational studies of line-of-sight velocity profile of ω Cen by Bianchini et al. (2013), which showed $V_{\text{max}} \approx 6 \text{ km s}^{-1}$ around $R = 500 \text{ arcsec}$. It is confirmed that the amplitudes of rations of the two populations are higher in the models with larger f_{rot} . However, the rotational amplitude is higher in the He-poor population than in the He-rich population for the simulated ω Cen in

these models. The models with larger f_{rot} show lower conversion efficiencies of gas to new (2G) stars (< 0.5) and the total mass of 2G stars in the models with $f_{\text{rot}} \geq 0.05$ are too low ($< 10^5 M_{\odot}$) to be consistent with the observed mass of He-rich stars (Norris 2004): this point is discussed in 3.2.4.

3.2.2. Radial abundance gradients

As shown in Figure 12, the slopes of radial abundance gradients (negative or positive) do not depend on model parameters for all but [Eu/Fe], though the details of the profiles (the central value) are different between different models. This is mainly because the formation of 2G star from AGB ejecta mixed with SNe II and NSM ejecta does not depend strongly on the model parameters. The positive slopes of [Eu/Fe] derived in some models are caused by the too large [Eu/Fe] of 2G stars formed from ICM polluted efficiently by NSM in the inner regions of these models. Since the details of mixing processes of NSM ejecta are not understood for ICM, the present study cannot make a robust conclusion as to whether the [Eu/Fe] radial gradient of simulated ω Cen should be negative or positive. It should be noted here that the observed [Eu/Fe] gradient appears to be weakly negative (Figure 9 of JP10), within the central 10 arcmin.

3.2.3. [X/Fe]–[Fe/H] relations

Although [X/Fe]–[Fe/H] relations are not so different between different models for X=C, N, O, Na, Mg, and Al, they depend strongly on the mixing process of NSM ejecta for Ba, La, and Eu, simply because they are produced efficiently by NSM. Figure 13 describes how the simulated [Eu/Fe]–[Fe/H] relation depends on r_{nsm} (search radius of NSM), $r_{\text{s},0}$ (stopping length), and f_{ret} (retention fraction of NSM ejecta). As shown in Figure 13 for the models with uniform mixing of NSM ejecta, if all NSM ejecta is retained ($f_{\text{ret}} = 1$) in a GC, then [Eu/Fe] can become too large (> 2) to be consistent with the observed [Eu/Fe]. Clearly, the simulated [Eu/Fe]–[Fe/H] relation is more consistent with the models with small f_{ret} (i.e., partial retention) than with those with $f_{\text{ret}} = 1$. It should be noted here, however, that all NSM ejecta is assumed to be mixed well with ISM with a mass of $\sim 10^6 M_{\odot}$ in theoretical studies for [Eu/Fe] evolution in galaxies (e.g., TS14). Such a 100% retention rate of NSM ejecta within ICM is highly unrealistic in forming GCs owing to the small amount of ICM ($< 10^6 M_{\odot}$). Thus, it is not a problem that the models with small f_{ret} can better reproduce the observation. In the density-dependent (“D”) models with larger r_{nsm} and larger $l_{\text{s},0}$, NSM ejecta can be mixed more uniformly for a wider region of ICM so that the net retention rates

of NSM ejects can become higher. Accordingly, these models do not show a strongly negative [Eu/Fe] at higher [Fe/H] (> -0.8) that is inconsistent with the observed slightly positive (JP10) or slightly negative [Eu/Fe] (S00, O11) for [Fe/H] > -0.8 .

As shown in Figure 14, the models with larger yields of La can better reproduce both the observed [La/Fe]–[Fe/H] and [Eu/Fe]–[Fe/H] relations for [Fe/H] > -0.8 . Since there is an uncertainty in theoretical predictions of chemical yields for La, it would not be unreasonable for the present study to use larger La yield for reproducing better the observations. Figure 14 also demonstrates that such models with larger yields of La can better explain the observed positive [La/Fe] at higher [Fe/H] (≈ -0.5). It should be noted here that the models with Y1 yield (i.e., lower La yield) do not show positive [La/Fe] at [Fe/H] ≈ -0.5 owing to the small [La/Fe] at [Fe/H] > -0.5 . The model with Y2 yield also show a small (≈ 0) [La/Fe] at [Fe/H] ~ -0.5 , which is not so consistent with observations (JP10). These low [La/Eu] at higher [Fe/H] can be seen for [Ba/Eu] in these models. These results strongly suggest that Ba and La yields should be larger than the predictions by F14 to reproduce the observed [Ba/Eu] and [La/Fe] at higher [Fe/H] in ω Cen.

3.2.4. Star formation efficiency for He-rich stars

The observed total mass of He-rich stars (10 – 20% of its total stellar mass ; Norris 2004) can be used as a key constraint on the IMF and the original mass of ω Cen (Bekki & Norris 2006). Although the fiducial model M1 shows that the total mass of He-rich stars with $Y > 0.25$ (M_{2g}) is $\sim 8 \times 10^5 M_\odot$, which is consistent with observations, some other models with different M_{gmc} , R_{gmc} , and r_{gmc} do not show such a large mass owing to the lower conversion (star formation) efficiency of the ICM (M13–M22). The models with larger f_{rot} (≥ 0.05) show $M_{2g} < 10^5 M_\odot$, because the the ICM has more extended spatial distributions and thus lower surface gas densities these models with larger initial angular momentum. This result combined with those of stellar kinematics depending on f_{rot} can allow us to narrow down the range of f_{rot} that can explain both the observed M_{2g} and V_{max} .

Furthermore, M_{2g} can be lower than $10^5 M_\odot$ in the models with lower M_{gmc} ($< 10^7 M_\odot$ for $f_{rot} = 0.01$). This result implies that there is a threshold GMC mass ($M_{gmc} \geq 10^7 M_\odot$) above which ω Cen can be formed with the right mass of 2G stars. The low-density GMC model with larger R_{gmc} ($= 280\text{pc}$) also shows a lower M_{2g} ($= 5.0 \times 10^5 M_\odot$ for $f_{rot} = 0.01$), which is lower than the observed mass of Y-rich stars. The model with $r_{gmc} = 500$ pc (i.e., located in the outer part of the dwarf’s galaxy) shows $M_{2g} = 3.3 \times 10^5 M_\odot$ that is significantly lower than that in the fiducial model with $r_{gmc} = 0$. It is confirmed that GMCs with such larger r_{gmc} show low star formation efficiencies in 2G formation. This suggests that the star

formation efficiency from ICM in a GC can be higher if the GC is located in the nuclear region of its host dwarf. The main reason for the higher star formation efficiency for $r_{\text{gmc}} = 0$ is that AGB ejecta can be more efficiently retained in the GC if it is located in the nuclear region.

4. Discussion

4.1. Short vs long formation timescales

The formation timescale of ω Cen in the present scenario (~ 300 Myr) is much shorter than those (more than a few Gyr) suggested by previous observational studies, which used different photometric and spectroscopic methods to derive the ages range: see Table 1 of the present study and Table 5 of Stanford et al. (2006) for a list of age ranges estimated for stellar populations of ω Cen in previous work done before 2006. The new short formation timescale can explain a number of the observed chemical abundance patterns of ω Cen, as demonstrated in §3. Furthermore, it is consistent with the observed low $[\text{Mn}/\text{Fe}]$ at $[\text{Fe}/\text{H}] \sim -1.0$ observed in ω Cen (Cunha et al. 2010). However, it has not been clearly explained in the present study how star formation can be almost truncated ~ 300 Myr after its formation. Massive ω Cen can have numerous AGB stars with lower masses ($\leq 3M_{\odot}$) even when it becomes older than 300 Myr. These AGB ejecta can be easily trapped by ω Cen (and by its host dwarf), and consequently it can be converted into new stars. However, if such AGB ejecta with rather high $[\text{Ba}/\text{Fe}]$ and $[\text{La}/\text{Fe}]$ (e.g., $[\text{La}/\text{Fe}] \sim 1.6$ and 2.1 for $m = 3M_{\odot}$ and $2M_{\odot}$, respectively; F14) is converted into new stars without dilution by pristine gas, then $[\text{Ba}/\text{Fe}]$ and $[\text{La}/\text{Fe}]$ can be too high to be consistent with observations.

Therefore, there should be a mechanism by which star formation can be truncated ~ 300 Myr after the formation of ω Cen. There are possible explanations for the origin of the sudden truncation of star formation. One is that SNe Ia in the central region of ω Cen can expel all of the remaining ICM to truncate further star formation: this idea was already discussed in D’Ercole et al. (2008). Since a fraction of SNe II ejecta can be retained by the central region of ω Cen’s host dwarf in the present models, this idea has need to explain why SNe Ia, whose explosion energy is similar to that of SNe II, can expel all of the remaining ICM within ω Cen. It seems that this idea is not so promising owing to the lack of a possible convincing mechanism for the removal of gas preferentially by SNe Ia (not by SNe II).

An alternative idea is that the host dwarf galaxy of ω Cen experiences strong ram pressure stripping of its ICM by the warm/hot halo gas of the Galaxy ~ 300 Myr after the formation of ω Cen. It is not clear, however, why ram pressure stripping can suddenly

become so efficient to remove the ICM around 300 Myr after the formation of ω Cen. One possible explanation is that ω Cen is formed in the first pericenter passage of its host dwarf with respect to the Galaxy (e.g., owing to rapid gas infall during galaxy interaction between the two) and then it loses ICM through ram pressure stripping in the second pericenter passage that is ~ 300 Myr after the first one. In this explanation, the pericenter distance of the host dwarf in the later multiple pericenter passages (2nd, 3rd, etc) should be significantly smaller than that of the first one so that ram pressure stripping is only effective in the later pericenter passages. If the host dwarf is massive enough to experience dynamical friction of the Galactic dark matter halo, then such a decreasing pericenter distance with increasing number of pericenter passages could be possible.

The main reason for the proposal of the short formation timescale of ω Cen is that there is no clear decrease of $[\alpha/\text{Fe}]$ with $[\text{Fe}/\text{H}]$ in observations (e.g., JP10). Although the number of stars used in JP10 (855) is large enough, a larger number of stars with $[\text{Fe}/\text{H}] > -0.8$ is required to confirm that there is no decrease of $[\text{Ca}/\text{Fe}]$, $[\text{Si}/\text{Fe}]$, and $[\text{Ti}/\text{Fe}]$ with increasing $[\text{Fe}/\text{H}]$ for $[\text{Fe}/\text{H}] > -0.8$, because the number of stars for that metallicity range is rather small in JP10. The decreasing trends of $[\text{Ba}/\text{Fe}]$, $[\text{La}/\text{Fe}]$, and $[\text{Eu}/\text{Fe}]$ with increasing $[\text{Fe}/\text{H}]$, which are the prediction of the present scenario, need to be confirmed in future observations with a much larger number of the investigated stars. It is beyond the scope of this paper how we can reinterpret the observational results of color magnitude diagrams (CMs) of ω Cen suggesting the long formation timescale (> 2 Gyr) in the context of the present scenario. A combination of photometric errors and differences in $[\text{Fe}/\text{H}]$, Y , and CNO abundances among stars could possibly broaden the distributions of the stars on the CM diagram thus mimic the large age spread.

4.2. Dependence on AGB yields

The present study has investigated the chemical abundances of stars in ω Cen based on only one AGB model (F14). It is therefore possible that the present results can be changed if AGB yields from other groups are incorporated into the adopted chemodynamical simulations of GC formation. We here discuss this point using the AGB yields from Ventura et al. (2013, V13), which have been used in chemical evolution studies of GCs with multiple stellar populations. One of differences between F14 and V13 is $[\text{O}/\text{Fe}]$ in stellar winds of massive AGB stars ($m \geq 6M_{\odot}$): it is ≈ -0.6 and -0.8 in F14 and V13, respectively. V13 also showed that the level of Mg-depletion in massive AGB stars with $m \approx [5 - 6]M_{\odot}$ ($[\text{Mg}/\text{Fe}] \approx -0.2$) is higher than that predicted in F14 ($[\text{Mg}/\text{Fe}] \approx 0.4$). Furthermore, $[\text{N}/\text{Fe}]$ in stellar winds of intermediate and massive AGB stars ($m \geq 5M_{\odot}$) are lower in V13 (ranging

from 1.4 to 1.6) than in F14 (from 1.8 to 2.5). Although C-depletion in ejecta from AGB stars with $m \geq 6M_{\odot}$ can be clearly seen in V13 ($-0.51 \leq [\text{C}/\text{Fe}] \leq -0.27$), it is not seen in F14: $[\text{C}/\text{Fe}]$ is as high as ≈ 1 for such a mass range.

These differences suggest that the following properties of the simulated ω Cen can change, if the AGB yield table by V13 is adopted in our chemodynamical simulations of GC formation. First, the mean $[\text{O}/\text{Fe}]$ of 2G stars in the simulated ω Cen can be lower than that derived in the present study, because the ICM is polluted by winds from massive AGB stars with smaller $[\text{O}/\text{Fe}]$. This means that the simulated $[\text{O}/\text{Fe}]$ – $[\text{Fe}/\text{H}]$ and $[\text{O}/\text{Na}]$ – $[\text{Fe}/\text{H}]$ relations (shown in Fig. 8) can be better fit to the corresponding observations (JP10). It is, however, clear that the observed stars with $[\text{O}/\text{Fe}] \approx -1$ (JP10) cannot be simply explained, even if V13 is adopted. Second, the radial gradient of $[\text{O}/\text{Fe}]$ can be slightly steeper owing to the lower $[\text{O}/\text{Fe}]$ in the central 2G population of the simulated ω Cen.

Third, the location of the peak in the $[\text{Mg}/\text{Fe}]$ distribution can be shifted toward a lower $[\text{Mg}/\text{Fe}]$ (by ≈ 0.2 dex at most) owing to the lower mean $[\text{Mg}/\text{Fe}]$ of 2G population. Fourth, the number fraction of stars with high $[\text{N}/\text{Fe}]$ (> 1) can be reduced owing to the lower $[\text{N}/\text{Fe}]$ of AGB ejecta in V13. Norris & Da Costa (1995) investigated the chemical abundances of 40 red giants in ω Cen and found $[\text{N}/\text{Fe}] < 1$ for almost all of them. Although Marino et al. (2011) found that stars with $[\text{Fe}/\text{H}] > -1.5$ have $[\text{N}/\text{Fe}] \approx 1.5$, there are no stars with $[\text{N}/\text{Fe}] > 1.8$. It is therefore possible that our future simulations with AGB yields from V13 ($[\text{N}/\text{Fe}] < 1.6$) will be able to reproduce better the observed $[\text{N}/\text{Fe}]$ abundances.

Fifth, the number fraction of stars with $[\text{C}/\text{Fe}] > 0.5$ among 2G stars can be decreased. The simulated ω Cen has a non-negligible fraction of stars with $[\text{C}/\text{Fe}] > 0.5$, which is not so consistent with the observational results by Norris & Da Costa (1995) and Marino et al. (2011), which showed almost all of the investigated stars show $[\text{C}/\text{Fe}] < 0.5$. Accordingly, adoption of AGB yields by V13 can improve the level of consistency between the observed and simulated $[\text{C}/\text{Fe}]$ distributions. Sixth, Y distributions and radial Y gradients cannot change significantly, because the predicted Y in AGB winds is not so different between F14 and V13. The lack of AGB yield table for $[\text{La}/\text{Fe}]$ and $[\text{Ba}/\text{Fe}]$ in V13 does not allow us to discuss how these abundance patterns can be changed in our chemodynamical simulations with the yields from V13.

4.3. The origin of global rotation

The present study has shown, for the first time, that (i) both He-poor and He-rich stars in ω Cen can have global rotation with respect to its center and (ii) the rotation amplitude

can be higher in the He-poor population. Our previous studies of GC formation, which do not include SN feedback effects of 2G stars on ICM, showed the higher amplitude of rotation in 2G stars that correspond to He-rich populations. Therefore, the above result (ii) implies that the number fraction of SNe II among 2G stars can possibly determine the stellar kinematics of 2G populations in GCs. Since ω Cen is massive enough to form high-mass stars that can explode as SNe II, the stellar kinematics of 2G stars can be significantly influenced by SNe II feedback effects (i.e., stirring of their host ICM) to have the lower amplitude of global rotation. On the other hand, GCs with lower masses cannot form SNe II progenitor stars so that the 2G stars can have more rotation than 1G stars owing to their dissipative formation from ICM.

The present study has also shown that the rotational energy of the natal GMC of ω Cen can control the present-day rotation amplitude of He-poor (1G) stars in ω Cen. The rotational kinematics of stars in typical GCs can be significantly changed during the long-term dynamical evolution of GCs driven by two-body relaxation (e.g., Mastrobuono-Battisti & Peters 2016). Although the long-term dynamical evolution of such a massive GC with at least two distinct populations with different kinematics is yet to be investigated (e.g., for GCs with lower masses), it cannot be so much changed for ω Cen with a long relaxation timescale. Therefore, it is reasonable to conclude that the observed V/σ in ω Cen can be used to infer the original f_{rot} of its natal GMC. Thus it is our future study to investigate whether the formation of a GMC with the suggested f_{rot} is possible in a dwarf galaxy at high z .

4.4. Was ω Cen really formed in a dwarf galaxy’s center ?

It has long been considered that ω Cen was the nucleus of a dwarf galaxy that had been completely destroyed by the Galaxy (e.g., Freeman 1993). The observed large metallicity spread of ω Cen was also considered to be observational evidence that supports this scenario, and the metallicity spread was suggested to be caused by repetitive gas infall to the nucleus over several Gyr in the early evolution of the host dwarf (e.g., BF03). As has been demonstrated in the present study, the origin of the observed wide range of [Fe/H] could not be due to the discrete star formation events due to repetitive gas infall to the nuclear region of ω Cen’s host dwarf over several Gyr suggested by BF03.

Formation of ω Cen in the nuclear region of its host dwarf has the following advantages in explaining the observed chemical abundances of ω Cen. First, the star formation efficiency from AGB ejecta can be quite high (~ 0.5), because almost all gas in AGB winds can be retained and consequently used for secondary star formation owing to the deep gravitational

potential well. Second, a significant amount of ICM polluted by SNe II can be also retained in the nuclear region so that it can be converted into new stars with higher $[\text{Fe}/\text{H}]$. Third, the stellar system composed largely of 1G stars does not lose the stars that can become AGB star to eject gas, because it does not suffer tidal stripping by its host. This can end up with the larger mass of 2G stars from AGB ejecta. Fourth, the existing field stars of the host galaxy could be gravitationally trapped by ω Cen to avoid tidal stripping during the final destruction of its host dwarfs. The field stars with low metallicities can be observed as the stars with $[\text{Fe}/\text{H}] < -1.8$ within ω Cen.

Thus, several properties of chemical abundances characteristic for ω Cen can be closely related to its formation in the nuclear region of a dwarf galaxy orbiting the early Galaxy. Such unique formation processes of ω Cen could also explain other physical properties of ω Cen. For example, the largest GC among the Galactic GC can be also explained by its formation in the host’s nuclear region, where a large amount of gas can be transferred to form a very massive GMC. A possible disadvantage of ω Cen formation in the nuclear region of its host is that star formation can continue in the deep potential well more than 300 Myr. A number of recent observational studies using the latest Gaia DR2 data have successfully discovered the tidal streams that can be associated with ω Cen (e.g., Ibata et al. 2019). It is our future study to construct a model which can reproduce not only the chemical and dynamical properties of ω Cen but also these latest proper motion results of the host dwarf galaxy.

4.5. Can the IMF of 2G stars in ω Cen distinguish it from other GCs ?

The present study has revealed that there are two unique physical processes that distinguish ω Cen from other “ordinary” GCs with no/little $[\text{Fe}/\text{H}]$ spread. One is the mixing of SNe II ejecta of 2G stars with AGB and NSM ejecta of 1G stars in the central region of ω Cen. The other is the efficient retention of such mixed ejecta in the central region for prolonged star formation. In order to form SNe II in 2G formation, the upper mass cut-off (m_{upp}) should be larger than $8M_{\odot}$ in the 2G formation of ω Cen. Our previous one-zone models of GC formation showed that 2G star formation can continue for $\sim 2 \times 10^8$ yr, if the IMF of stars in 2G formation is top-light with the upper mass cut-off (m_{upp}) less than $8M_{\odot}$ (Bekki et al. 2017, BJK17). This is mainly because 2G formation cannot be truncated by the energetic feedback effects of SNe II (i.e., no SNe II). The lack of chemical enrichment by SNe II in 2G formation ends up with no $[\text{Fe}/\text{H}]$ spreads among 2G stars.

Accordingly, it is possible that the IMF in 2G formation can be a crucial factor that distinguishes between ω Cen and other ordinary GCs with multiple stellar populations yet

no/little [Fe/H] spreads. In such a massive GC as ω Cen, m_{upp} can be larger than $8M_{\odot}$ owing to the higher star formation rate of 2G stars (BJK17): however, it should not be so large ($< 20M_{\odot}$) so that the mass fraction of SNe II (f_{sn2}) can be low to have 2G stars with the maximum [Fe/H] as low as -0.3 : high f_{sn2} can end up with the formation of new stars with [Fe/H] ≈ 0 , which is not observed. On the other hand, m_{upp} can be lower than $8M_{\odot}$ owing to the lower star formation rate of 2G stars in ordinary GCs. Therefore, the mass-density of ICM, which can determine the IMF of 2G stars (e.g., Marks et al. 2012), can be a key factor that distinguishes between ω Cen and other ordinary GCs. The ICM of forming ω Cen can possibly have a high mass-density owing to (i) its original large mass and (ii) its formation in the central region of its host dwarf.

4.6. Unresolved problems and future works

Although the present study has demonstrated that some of the observed properties of ω Cen can be explained by the new model with the short formation timescale, it cannot explain a number of key observations of ω Cen in a fully self-consistent manner. First, it is not clear why there are 15 distinct populations with possibly different Y , [N/Fe] and [Fe/H] in ω Cen (see Table 1 in Bellini et al. 2017). The present study has shown that there are three peaks in the Y distribution of the simulated ω Cen, which means that the GC has three distinct populations. Although the simulated ω Cen has a wide range of [Na/Fe], several distinct peaks in the [N/Fe] have not been found in the present study, which is not so consistent with observational results by Bellini et al (2018). The star formation processes in the present study are not discrete events so that the observed large number of distinct populations cannot be simply explained by the present models. It has been demonstrated that such discrete star formation events can be possible if each star formation event is completely truncated by its SNe II (Bekki et al. 2017). However, such complete truncation of star formation does not occur in the present models.

Second, the mass-ratio of metal-poor 1G ([Fe/H] ≈ -1.7) to metal-rich 2G stars ([Fe/H] > -1.5) is a bit too large (> 10): the simulated [Fe/H] distribution has a too strong peak around [Fe/H] ~ -1.7 whereas the observed one shows multiple distinct peaks (e.g., Figure 7 in JP10). The inability of the present models to reproduce the observed significant fraction of more metal-rich stars is due partly to the large original mass of 1G stars in the simulated ω Cen ($\sim 10^7 M_{\odot}$). Although ω Cen can lose a significant fraction of its 1G stars during its tidal interaction with the Galaxy, it can lose at most 70% of its original mass to match the observed present-day total mass ($\approx 3 \times 10^6 M_{\odot}$ in 1G). Therefore, other mechanism(s) is required to explain the large fraction of 1G stars that are observed to be centrally concentrated within

10 arcmin of ω Cen. One possible idea is that the IMF of 1G stars from its natal GMC is top-heavy to increase the number of AGB stars thus the total mass of AGB ejecta from which 2G stars can be formed. Such a top-heavy IMF can also decrease the number of low-mass stars ($m < 0.8M_{\odot}$) that can be observed in the present-day ω Cen. Recent theoretical models for IMFs have shown that the IMF in GC formation should be top-heavy to explain the mass function of low-mass stars in GCs (e.g., Marks et al. 2012). Therefore, this idea of top-heavy IMF is promising and worth an investigation in our future study to resolve this problem.

Third, the details of the mixing processes of NSM ejecta is not fully understood in the formation of ω Cen. There are still two unknown parameters that describe the processes, i.e., the stopping length (l_s) and the retention fraction of the ejecta (f_{ret}). Although the present study has demonstrated that some models with a particular range of these two parameters can reproduce the observed $[\text{Eu}/\text{Fe}] - [\text{Fe}/\text{H}]$ relation, the physical processes that control r_s and f_{ret} are yet to be understood fully. We will need to perform high-resolution hydrodynamical simulations that are specially focused on the evolution of ICM surrounding one NSM event in order to quantify how the two parameters depend on the physical properties of ICM such as the density, total mass, and magnetic field. Fourth, the details of the internal stellar kinematics of ω Cen are yet to be fully explained by the present study, which has discussed only the global rotation of He-poor and He-rich populations. The velocity dispersion dependent on stellar masses and the orbital anisotropy of stars in ω Cen have been recently revealed (e.g., Bellini et al. 2018; Jindal et al. 2019). Since the present study did not investigate the long-term dynamical evolution of ω Cen, it cannot discuss these latest observations in a quantitative way. It is accordingly our future dynamical study to reproduce these observations in the context of the present new scenario of ω Cen.

Finally, the observed low $[\text{Rb}/\text{Zr}]$ (~ -0.5) over a wide range of $[\text{Fe}/\text{H}]$ in ω Cen (e.g., S00) cannot be simply explained by the present model with a short formation timescale. Such a low $[\text{Rb}/\text{Zr}]$ of -0.5 in S00 was suggested to be consistent with chemical enrichment by low-mass AGB stars ($m < 3M_{\odot}$) and thus with a long star formation timescale. Indeed the latest stellar yields of $[\text{Rb}/\text{Zr}]$ for AGB stars from Karakas et al. (2018) are larger than -0.063 for $m > 4M_{\odot}$, which is significantly larger than the observed values by S00. There are two possible ways to solve this discrepancy in the context of the present short formation timescale. One is to consider that low-mass AGB models with enhanced Y , which correspond to 2G stars in the present study, will evolve more than twice as fast (e.g., Karakas et al. 2014). Accordingly, it is possible that 2G He-rich low-mass AGB stars ($m \sim 2.4M_{\odot}$) whose lifetimes can be as short as 200 Myr can enrich ICM with their ejecta with low $[\text{Rb}/\text{Zr}]$ even in the ~ 300 Myr formation timescale of ω Cen. New stars formed from such ejecta from He-rich low-mass AGB stars (mixed with SNe II ejecta) can show low $[\text{Rb}/\text{Zr}]$, though it is

not clear whether the observed low $[\text{Rb}/\text{Zr}]$ over a wide range of $[\text{Fe}/\text{H}]$ can be reproduced.

The other is that the field low-mass AGB stars in the ω Cen’s host dwarf galaxy can chemically pollute the ICM of ω Cen owing to the trapping of the gaseous ejecta by the dwarf itself. In this idea, the ω Cen’s host GMC was formed well after the formation of its host dwarf galaxy. This idea is promising, as long as the AGB ejecta of the field stars can be retained within the central < 30 pc of ω Cen (i.e., not just by the dwarf itself). This means that if the dwarf galaxy is a rotating disk, then the gas ejected from the field stars need to lose a large amount of angular momentum so that it can be funneled to the inner < 30 pc of ω Cen (classic “fueling” problem). If the dwarf is a spheroid dynamically supported by random motion of stars, then such a fueling problem would not occur. Furthermore, the right amount of gas ejected from the AGB stars needs to be required to lower $[\text{Rb}/\text{Zr}]$ from 0 in the ICM to the observed -0.5 . The required large amount of ejecta of low-mass AGB stars with normal Y can lower Y of ICM to end up with the formation of 2G stars with normal Y – which would not be consistent with high Y of 2G stars in ω Cen. Thus the idea of short evolution of He-rich AGB stars appears to be more promising and thus worth a detailed investigation in our future studies. It should be finally noted here that the average $[\text{Rb}/\text{Zr}]$ for three stars of ω Cen observed by Vanture et al. (1994) is 0.2.

5. Conclusions

We have adopted a new formation scenario of the Galactic GC ω Cen and thereby investigated the chemodynamical evolution of ω Cen using our original hydrodynamical simulation code with chemical enrichment and feedback effects from Type II supernovae (SNe II) and asymptotic giant branch (AGB) stars and a new retention model of ejecta from neutron star mergers (NSMs). In the scenario, ω Cen was formed from a giant molecular cloud (GMC) in the central region of an ancient dwarf galaxy that was accreted onto the Galaxy. The nuclear GC could become ω Cen after its host galaxy was completely destroyed by the tidal field of the Galaxy. A key element of the scenario is that ω Cen was formed from a GMC within ~ 300 Myr, which is much shorter than those assumed in previous studies. We have derived chemical abundances of various elements (e.g., He, C, N, O, Mg, Al, Ba, La) from the simulated GC and the spatial variations of these within the GC (e.g., radial gradient of chemical abundances). We have briefly discussed how the results can change, if we adopt different yield tables of AGB stars and SNe II from other groups (e.g., V13). The principal results are as follows:

- (1) After the bursty formation of first generation (1G) of stars from the original GMC, second generation (2G) of stars can be later formed from gas that is ejected from 1G AGB

stars. A significant fraction of 2G stars can have higher He abundances (Y) and higher $[\text{Fe}/\text{H}]$, because AGB ejecta from 1G can be polluted by SNe II yet can be retained in the central region of the GC’s dwarf for secondary star formation. The He-rich (2G) stars are more strongly concentrated in the central region of the GC in comparison with He-poor (1G) stars, and this result does not depend on model parameters. The simulated ω Cen initially has a flattened shape and the He-rich population ($Y > 0.25$) shows a slightly more flattened shape than the He-poor population ($Y < 0.25$). The simulated ω Cen has a negative radial gradient of Y with the slope of -0.003 pc^{-1} within the central 10 pc, and this result does not depend on model parameters.

(2) The simulated ω Cen shows a small amplitude of rotation ($< 5 \text{ km s}^{-1}$) in its He-poor population, and the rotational amplitude depends strongly on the initial ratio of rotational energy to total kinetic energy in its natal GMC. The observed rotational amplitude of ω Cen can be better reproduced by the models with $f_{\text{rot}} \sim 0.03$ for the adopted virial ratios of GMCs. He-rich population show a less amount of rotation, because it is formed from gas mixed with SNe II ejecta. The smaller amplitude of rotation in He-rich (mostly 2G) stars in the present study is therefore in a striking contrast with previous simulations in which 2G stars are formed from AGB ejecta without mixing with SNe II ejecta.

(3) The GC stars have bimodal number distributions in $[\text{C}/\text{Fe}]$, $[\text{N}/\text{Fe}]$, $[\text{O}/\text{Fe}]$, and $[\text{Na}/\text{Fe}]$ owing to the formation of 2G stars from AGB ejecta. For example, new stars formed from AGB ejecta mixed with SNe II ejecta have rather low $[\text{O}/\text{Fe}]$ (< 0) and higher $[\text{Fe}/\text{H}]$ whereas those formed from original gas polluted by SNe II ejecta (that is not well mixed with AGB ejecta) have higher $[\text{O}/\text{Fe}]$ and higher $[\text{Fe}/\text{H}]$. This bimodal $[\text{O}/\text{Fe}]$ distribution in the simulated GC can be seen in the observed $[\text{O}/\text{Fe}]$ distribution for ω Cen (e.g., JP10). The simulated ω Cen does not show clear bimodal distributions in $[\text{Mg}/\text{Fe}]$ and $[\text{Al}/\text{Fe}]$.

(4) Negative radial gradients (i.e., higher abundances for inner regions) of $[\text{Fe}/\text{H}]$, $[\text{C}/\text{Fe}]$ and $[\text{N}/\text{Fe}]$ can be seen in the simulated ω Cen, however, such gradients cannot be clearly seen in $[\text{O}/\text{Fe}]$, $[\text{Na}/\text{Fe}]$, $[\text{Mg}/\text{Fe}]$ and $[\text{Al}/\text{Fe}]$. The simulated negative $[\text{Fe}/\text{H}]$ gradient is not clearly observed (JP10), which implies that the long-term dynamical evolution of the GC should wipe out the original gradient to explain the observation. There is a weak positive radial gradient for $[\text{O}/\text{Fe}]$ in some models of the present study. The lower $[\text{O}/\text{Fe}]$ in the central region of the GC is due to the accumulation of massive AGB ejecta in the central region where new stars can be formed. Since these positive or negative radial abundance gradients are not so strong even in the early phase of ω Cen formation, they could be wiped out over $\sim 10 \text{ Gyr}$ due to the long-term two-body relaxation processes of ω Cen.

(5) The distribution of stars on the $[\text{N}/\text{Fe}]-Y$ plane (“chromosome map”) for simulated ω Cen shows a wide range of $[\text{N}/\text{Fe}]$ from ~ 0 to ~ 1.5 for each of the three major popu-

lations with different Y . This is mainly because AGB ejecta with high Y and high $[\text{N}/\text{Fe}]$ can mix with SNe II ejecta with high Y and very low $[\text{N}/\text{Fe}]$ (~ -0.8) to different degrees in different local star-forming regions. The distributions of stars on the $[\text{O}/\text{Fe}]$ – $[\text{Fe}/\text{H}]$ and $[\text{O}/\text{Na}]$ – $[\text{Fe}/\text{H}]$ planes for simulated ω Cen have a bimodality, though they are rather complicated. However the details of the distributions are not so consistent with corresponding observations owing to the presence of a large number of stars with large $[\text{O}/\text{Fe}]$ (> 0.5), as long as K06 is adopted for $[\text{O}/\text{Fe}]$ in SNe II. These $[\text{O}/\text{Fe}]$ – $[\text{Fe}/\text{H}]$ and $[\text{O}/\text{Na}]$ – $[\text{Fe}/\text{H}]$ relations can be changed, if AGB yields from other groups (e.g., V13) are incorporated into the present simulations, because $[\text{O}/\text{Fe}]$ in stellar winds of AGB stars is different between different groups. The lower $[\text{O}/\text{Fe}]$ predicted for massive AGB stars in V13 implies that the relations can be better reproduced, if their AGB yields are adopted in the present study.

(6) The chemical abundances of s -process elements, $[\text{La}/\text{Fe}]$ and $[\text{Ba}/\text{Fe}]$, rapidly increase around $[\text{Fe}/\text{H}] \sim -1.5$ in the early formation phase of ω Cen owing to star formation from gas ejected from AGB stars. However, $[\text{La}/\text{Fe}]$ and $[\text{Ba}/\text{Fe}]$ soon decrease with increasing $[\text{Fe}/\text{H}]$, mainly because 2G SNe II can heavily pollute the intra-cluster medium (ICM) from which new stars are formed. The simulated ω Cen shows rather weak negative gradient of $[\text{La}/\text{Fe}]$ and $[\text{Ba}/\text{Fe}]$, in particular, within the central few pc. The $[\text{La}/\text{Fe}]$ and $[\text{Ba}/\text{Fe}]$ number distributions show weak second peaks around $[\text{La}/\text{Fe}]$ and $[\text{Ba}/\text{Fe}] \approx 0.5$, though the bimodal distributions are not so clear as $[\text{O}/\text{Fe}]$ and $[\text{Na}/\text{Fe}]$. The efficient trapping of AGB ejecta and the partial retention of NSM ejecta cooperate to increase $[\text{La}/\text{Eu}]$ from -0.6 to 0.6 for $-1.7 < [\text{Fe}/\text{H}] < -1.5$. This difference in the retention capabilities between AGB and NSM ejecta is the essential factor for the observed $[\text{La}/\text{Fe}]$ – $[\text{Fe}/\text{H}]$ relation in ω Cen, because full retention of NSM ejecta can dramatically decrease $[\text{La}/\text{Eu}]$.

(7) NSMs both from 1G and 2G stars play a significant role in the evolution of $[\text{Eu}/\text{Fe}]$, because NSM ejecta can be partially trapped and retained in ICM of the forming GC owing to the rather high gas density of the ICM. Ejection of r -process elements (e.g, Eu) can temporarily increase $[\text{Eu}/\text{H}]$ to a large extent within the early formation phase of the GC. 2G SNe II can decrease $[\text{Eu}/\text{Fe}]$ of the ICM due to Fe ejection whereas NSMs can increase $[\text{Eu}/\text{Fe}]$ later. Therefore, the time evolution of $[\text{Eu}/\text{Fe}]$ depends strongly on (i) the formation rates of SNe II and NSMs and (ii) the retention capability of these ejecta by ICM in the GC. The fiducial model shows a decreasing $[\text{Eu}/\text{Fe}]$ with increasing $[\text{Fe}/\text{H}]$, which is consistent with some observations (e.g., D11) yet inconsistent with JP10 showing an almost constant $[\text{Eu}/\text{Fe}]$ over a wide range of $[\text{Fe}/\text{H}]$. The present study can reproduce well the presence of some stars with unusually low $[\text{Eu}/\text{Fe}]$ (< 0) observed in ω Cen.

(8) The moderately wide range of $[\text{Fe}/\text{H}]$ observed in ω Cen can be reproduced only if the IMF of 2G stars is top-light (i.e., a smaller number of massive stars that explode as

SNe II). If a canonical IMF is adopted for 2G stars, then the most metal-rich stars can be too metal-rich ($[\text{Fe}/\text{H}] > 0$), though the number is small. Although the total mass of He-rich stars in the simulated ω Cen ($\sim 7 \times 10^5 M_\odot$) is consistent with observation, the mass fraction of He-rich and metal-rich 2G stars (< 0.1) is smaller than the observed fraction (≈ 0.2). This problem can be mitigated if the total mass of 1G stars becomes much smaller owing to (i) selective stripping of 1G stars from the GC during its merging with the Galaxy or (ii) the top-heavy IMF of 1G stars.

(9) The observed flattened shape of ω Cen can be due to the angular momentum of its natal GMC formed in the central region of its host dwarf galaxy. The formation process of such a massive GMC in the dwarf is beyond the scope of this paper. The global rotation of the GMC is responsible for the formation of 1G population with a significant amplitude of rotation, and such rotation of 1G population and SNe II feedback effects combine to control the rotational amplitude of 2G population in the GC. It is our future study to investigate the long-term dynamical evolution of these initially rotating populations of the GC orbiting the Galaxy.

(10) Although the present model can explain at least qualitatively some of the observed characteristic features in the chemical abundance patterns of ω Cen, the level of consistency between observations and simulations is far from satisfactory. For example, the simulated distributions of stars on the $[\text{N}/\text{Fe}]$ – Y , $[\text{O}/\text{Fe}]$ – $[\text{Fe}/\text{H}]$, and $[\text{O}/\text{Na}]$ – $[\text{Fe}/\text{H}]$ maps are not so consistent with observations. Also, it is found to be very difficult for the present simulation to identify ~ 15 distinct subpopulations observed in ω Cen, because the formation of 2G stars in the simulation is not discrete. These problems will need to be addressed in our future simulations with more sophisticated modeling of mixing of SNe II, AGB, and NSM ejecta and metallicity-dependent chemical yields and stellar evolution (e.g., evolution of He-rich AGB stars).

(11) Thus, a number of unique physical processes in ω Cen formation can be responsible for the observed properties that are distinguished from those of other ordinary GCs with multiple stellar populations yet without $[\text{Fe}/\text{H}]$ spreads. ω Cen is the crossroad of astrophysical processes in the sense that its unique properties reflect various physical processes involved in its formation: Table 6 presents a brief summary of these processes. For example, the partial retention of NSM ejecta and efficient mixing of SNe II, AGB, and NSM ejecta cooperate to cause the observed unusually low $[\text{Eu}/\text{Fe}]$ (< 0) at $[\text{Fe}/\text{H}] > -1$ and rather high $[\text{La}/\text{Eu}]$ at $[\text{Fe}/\text{H}] \sim -1.5$ in ω Cen. Its chemical enrichment due predominantly to SNe II (not SNe Ia) over a short period (~ 300 Myr) has something to do with the unique formation processes of stars (e.g., top-light IMF and the longer minimum delay time of SNe Ia). Given that the present study has not successfully explained a few of the observed properties of ω

Cen so well, some new physical processes will need to be included in our future simulations of ω Cen formation.

We are grateful to the referee for constructive and useful comments that improved this paper.

REFERENCES

- Anderson, J., 1997, PhD Thesis, UC, Berkeley
- Bedin, L. R., 2004, *ApJL*, 605, 125
- Bastian, N., Lardo, C., 2018, *ARA&A*, 56, 83
- Bekki, K., 2006, *MNRAS*, 367, L24
- Bekki, K., 2011, *MNRAS*, *MNRAS*, 412, 2241
- Bekki, K., 2013, 432, 2298 (B13a)
- Bekki, K., 2013, 436, 2254 (B13b)
- Bekki, K., 2017a, *MNRAS*, 467, 1857 (B17a)
- Bekki, K., 2017b, *MNRAS*, 469, 2933 (B17b)
- Bekki, K., 2019, *MNRAS*, 486, 2570 (B19a)
- Bekki, K., 2019, *A&A*, 622, 53 (B19b)
- Bekki, K., Freeman, K. C., 2003, *MNRAS*, 346, L11 (BF03)
- Bekki, K., Chiba, M., 2007, *ApJ*, 665, 1164
- Bekki, K., Campbell, S. W., Lattanzio, J. C., Norris, J. E., 2007, *MNRAS*, 377, 335 (B07)
- Bekki, K., Yong, D., 2012, *MNRAS*, 419, 2063
- Bekki, K., Tsujimoto, T., 2016, *ApJ*, 831, 70
- Bekki, K., Tsujimoto, T., 2017, *ApJ*, 844, 34 (BT17)
- Bekki, K., Jerabkova, T., Kroupa, P., 2017, *MNRAS*, 471, 2242

- Bergin, Edwin A.; Tafalla, M., 2008, *ARA&A*, 2007, 45, 339
- Bellini, A., et al., 2017, *ApJ*, 842, 7
- Bellini, A., et al., 2018, *ApJ*, 853, 86
- Bianchini, P., et al. 2013, *ApJ*, 772, 67
- Bono, G., et al. 2019, *ApJ*, 870, 115
- Busso, M., et al., 2001, *ApJ*, 557, 802
- Carraro, G., Lia, C., 2000, *A&A*, 357, 977
- Cunha, K., et al., 2010, *ApJ*, 717, 333
- D’Antona, F., & Caloi, V. 2004, *ApJ*, 611, 871
- D’Antona, F., et al., 2011, *ApJ*, 736, 5
- D’Ercole, A., Vesperini, E., D’Antona, F., McMillan, S. L. W., & Recchi, S. 2008, *MNRAS*, 391, 825
- Dinescu, D. I., et al. 1999, *AJ*, 117, 277
- D’Orazi, V., et al. 2011, *A&A*, 534, 29 (D11)
- Dominik et al. 2012, *ApJ*, 759, 52
- Ferraro, F., et al., 2004, *ApJL*, 603, 81
- Fishlock, C. K., et al., 2014, *ApJ*, 797, 44
- Freeman, K., & Rodgers, A. W., 1975, *ApJ*, 201, 71
- Freeman, K., 1993, in Smith G. H., Brodie J. P., eds, *ASP Conf. Ser. Vol. 48, The Globular Clusters-Galaxy Connection*. Astron. Soc. Pac., San Francisco, p. 608
- Gnedin, O. Y., et al., 1999, 522, 935
- Gratton, R. G., et al. 2011, *A&A*, 534, 72
- Hilker, M., Richtler, T., 2000, *A&A*, 362, 895
- Hughes, J., Wallerstein, G., 2000, *AJ*, 119, 1225
- Ibata, R. A., et al., 2019, *NatAs*, 258

- Ideta, et al., 2004, ApJL, 616, 107
- Ikuta, C., Arimoto, N., 2000, A&A, 358, 535
- Jindal, et al., 2019, preprint (arXiv190311070)
- Johnson, C. I., Pilachowski, C. A., 2010, ApJ, 722, 1373 (JP10)
- Karakas, A. I., et al., 2014, ApJ, 784, 32
- Karakas, A. I., et al., 2018, MNRAS, 477, 421
- Kobayashi, C., et al. 2006, ApJ, 653, 1145 (K06)
- Lee, Y.-W., et al., 1999, Nature, 402, 55
- Lee, Y.-W., et al. 2002, Extragalactic Star Clusters, IAU Symposium 207, Eited by D. Geisler, E.K. Grebel, and D. Minniti. San Francisco., Astronomical Society of the Pacific, p.110
- Magurno, D., et al. 2019, preprint, arXiv:1906.08550
- MaKenzie, M., Bekki, K., 2018, MNRAS, 479, 3126
- Marcolini, A., et al., 2007, MNRAS, 382, 443
- Marino, A. F., Milone, A. P., Piotto, G., Villanova, S., Bedin, L. R., Bellini, A., Renzini, A., 2009, A&A, 505, 1099
- Marino, A. F., et al., 2011, ApJ, 731, 64
- Marino, a., et al. 2019, in preprint (arXiv190405180)
- Marks, M., et al. 2012, MNRAS, 422, 2246
- Mastrobuono-Battisti, A., Perets, H. B., 2016, ApJ, 823, 61
- Meylan, G., 1987, A&A, 184, 144
- Meylan, G., Mayor, M., Duquennoy, A., Dubath, P., 1995, A&A, 303, 761
- Mizutani, A., et al, 2003, ApJL, 589, 89
- Myeong, G. C., et al., 2018, MNRAS, 478, 5449
- Norris, J. E., 2004, ApJL, 610, 25

- Norris, J. E., & Da Costa, G. S., 1995, *ApJ*, 447, 680
- Origlia, L., et al. 2003, *ApJ*, 591, 916
- Pancino, E., et al., 2002, *ApJL*, 568, 101
- Pancino, E., et al., 2011, *A&A*, 527, 18
- Phillips, J. P., 1999, *A&AS*, 134, 241
- Piotto, G., et al., 2005, 621, 777
- Prantzos, N., Charbonnel, C., 2006, *A&A*, 458, 135
- Renzini, A., et al., 2015, *MNRAS*, 454, 4197
- Rey, S-C., et al. 2000, *AJ*, 119, 1824
- Romano, D., et al., 2007, *MNRAS*, 376, 405
- Romano, D., et al., 2011, *MNRAS*, 418, 696
- Rosolowsky, E., Engargiola, G., Plambeck, R., Blitz, L., 2003, *ApJ*, 599, 258
- Siegel, D. M., Barnes, J., Metzger, B. D., 2019, *Nature*, 569, 241
- Simmerer, J., et al. 2004, *ApJ*, 617, 1091
- Smith, V., et al. 2000, *AJ*, 119, 1239 (S00)
- Sollima, A., et al., 2005, *MNRAS*, 357, 265
- Sollima, A., et al., 2007, *ApJ*, 654, 915
- Stanford, L. M., et al. 2006, *ApJ*, 647, 1075
- Sutherland R. S., Dopita M. A. 1993, *ApJS* 1993, 88, 2531
- Tominaga, N., Umeda, H., Nomoto, K., 2007, *ApJ*, 660, 516
- Totani, T., et al. 2008, *PASJ*, 60, 1327
- Tsujimoto, T., & Shigeyama, T., 2003, *ApJ*, 590, 803
- Tsujimoto, T., & Bekki, K., 2012, *ApJ*, 747, 125
- Tsujimoto, T., & Shigeyama, T., 2014, *ApJ*, 795, L18 (TS14)

Tsujimoto, T., Yokoyama, T., & Bekki, K. 2017, *ApJ*, 835, L3

Vanture, A. D., et al., 1994, *PASP*, 106, 835

Ventura, P., et al. 2013, *MNRAS*, 431, 3642 (V13)

Vesperini, E., McMillan, S. L. W., D’Antona, F., & D’Ercole, A. 2010, *ApJ*, 718, L112

Villanova, S., et al. 2007, *ApJ*, 663, 296

Wylie de-Boer, E., et al., 2010, *AJ*, 139, 636

Table 4. Description of the values of major parameters for the representative models.

ID ^a	M_{gmc} ^b	R_{gmc} ^c	f_{rot} ^d	r_{gmc} ^e	Yield ^f	Mixing ^g	r_{nsm} ^h	$l_{\text{s},0}$ ⁱ	f_{ret} ^j
M1	2	140	0.01	0	Y3	D	2.7	0.78	–
M2	2	140	0.01	0	Y1	D	2.7	0.78	–
M3	2	140	0.01	0	Y2	D	2.7	0.78	–
M4	2	140	0.01	0	Y4	D	2.7	0.78	–
M5	2	140	0.01	0	Y1	D	2.7	0.26	–
M6	2	140	0.01	0	Y1	D	2.7	2.6	–
M7	2	140	0.01	0	Y1	D	2.7	26.0	–
M8	2	140	0.01	0	Y1	D	0.27	26.0	–
M9	2	140	0.01	0	Y1	U	5.0	–	0.01
M10	2	140	0.01	0	Y4	U	5.0	–	0.01
M11	2	140	0.01	0	Y1	U	30.0	–	1.0
M12	2	140	0.01	0	Y1	U	5.0	–	1.0
M13	2	140	0.03	0	Y3	D	2.7	0.78	–
M14	2	140	0.05	0	Y3	D	2.7	0.78	–
M15	2	280	0.01	0	Y3	D	2.7	0.78	–
M16	2	140	0.01	40	Y3	D	2.7	0.78	–
M17	2	140	0.01	100	Y3	D	2.7	0.78	–
M18	2	140	0.01	200	Y3	D	2.7	0.78	–
M19	2	140	0.01	500	Y3	D	2.7	0.78	–
M20	2	140	0.01	1000	Y3	D	2.7	0.78	–
M21	1	140	0.01	0	Y3	D	2.7	0.78	–
M22	6	140	0.01	0	Y3	D	2.7	0.78	–

^a M1 corresponds to the fiducial model.

^b The initial total mass of a GMC in units of $10^7 M_{\odot}$.

^c The initial radius of a GMC in units of pc.

^d The initial fraction of rotational energy among total kinetic energy in a GMC.

^e The initial position of a GMC from the center of its host dwarf galaxy in units of pc.

^f Yield models for AGB ejecta. The yield table is given in Table 2.

^g Mixing model for NSM ejecta. “D” and “U” represent the density-dependent and uniform models, respectively.

^h The search radius (pc) for neighboring gas particles around a NSM event.

ⁱ The stopping length (pc) for the reference gas density ($10^5 \text{ atom cm}^{-3}$).

^j The retention fraction of NSM ejecta for the uniform mixing model.

Table 5. Observational diagnostics for the present new model of ω Cen with a short formation timescale (~ 300 Myr). If observations are well reproduced by the present model, “ \checkmark ” are given. If they are not reproduced by the present model, and if there are promising ways to resolve this inconsistency, “ \triangle ” are given. If observations are not reproduced by the present model, and if there are no promising solutions for them, “ \times ” are given.

Item	Consistency	Comments
Flattened shape	\checkmark	
Global rotation	\checkmark	Higher f_{rot} required
Large [Fe/H] dispersion	\checkmark	
He-rich, metal-rich population	\checkmark	
Populations with different Y	\checkmark	
Radial gradient of Y	\checkmark	
Bimodal [O/Fe] distribution	\checkmark	
Fraction of O-poor stars	\checkmark	
Central concentration of O-poor stars	\checkmark	
Wide abundance ranges for C, N and Na	\checkmark	
Stellar distribution on [N/Fe]– Y	\triangle	
Stellar distribution on [O/Na]–[Fe/H]	\times	Some stars with [O/Na] > 0
Relation between [Ba/Fe] and [Fe/H]	\triangle	Peak at lower [Fe/H] (~ -1.5)
Relation between [La/Fe] and [Fe/H]	\triangle	Peak at lower [Fe/H] (~ -1.5)
Relation between [Eu/Fe] and [Fe/H]	\checkmark	
Higher [La/Eu] at [Fe/H] ~ -0.5	\checkmark	Larger La yield required
Low [Rb/Zr]	\times	Shorter lifetimes of He-rich stars ?
Distinct 15 subpopulations	\times	

Table 6. A brief summary for the unique physical processes in ω Cen formation that are responsible for its observed characteristics. These processes that are investigated in this work and will be done in future works are separately listed in this table.

Physical process	Relevant observed properties
Present work	
(1) Retention and mixing of SNe II ejecta in ICM	A wide range of [Fe/H]
(2) Star formation from AGB ejecta mixed with SNe II	He-rich populations with higher [Fe/H]
(3) 2G formation preferentially in the central region	Negative radial gradient of Y
(4) Top-light IMF in 2G formation	Efficient 2G formation
(5) No/little dilution of AGB ejecta by ISM	Stars with very low [O/Na] (< -0.6)
(6) Full (partial) retention of AGB (NSM) ejecta	Sharp rise of [La/Eu] from [Fe/H] ~ -1.6
(7) No/little contribution of SNe Ia	No/little evolution of $[\alpha/\text{Fe}]$
(8) Partial retention of NSM ejecta	Unusually low [Eu/Fe] (< 0)
(9) Global rotation of the natal GMC	Rotation of Y -poor stars
Future work	
(10) Star formation truncation by gas stripping	Short formation timescale of ω Cen
(11) Time-evolving IMF in 2G formation	Zone of avoidance in [Na/O]-[Fe/H] map
(12) Evolution of He-rich AGB stars	Low [Rb/Zr]
(13) Discrete star formation events	15 subpopulations
(14) Formation of massive GMC in a dwarf	The origin of its unusually large mass
(15) Accretion of its host dwarf	Retrograde orbit around the Galaxy

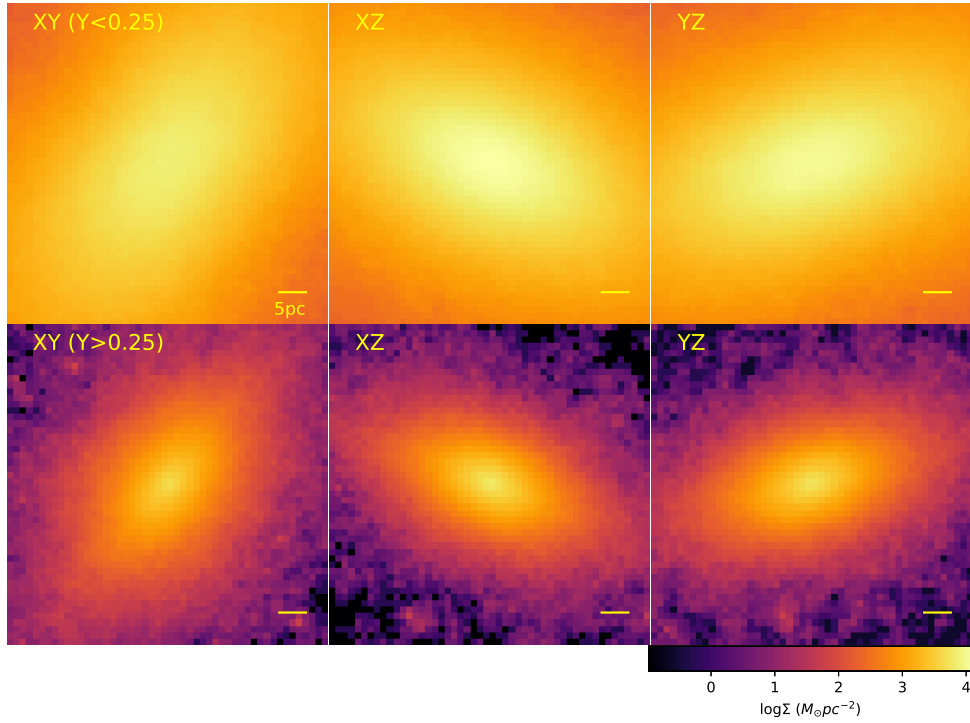


Fig. 1.— Mass distributions of “He-poor” ($Y \leq 0.25$, upper) and “He-rich” ($Y > 0.25$, lower) stars projected onto to the x - y (left), x - z (middle), and y - z (right) planes for the simulated ω Cen at the final time step ($T = 298$ Myr) in the fiducial model M1. The surface mass density is estimated at each mesh point and shown in these 2D maps with 50×50 meshes.

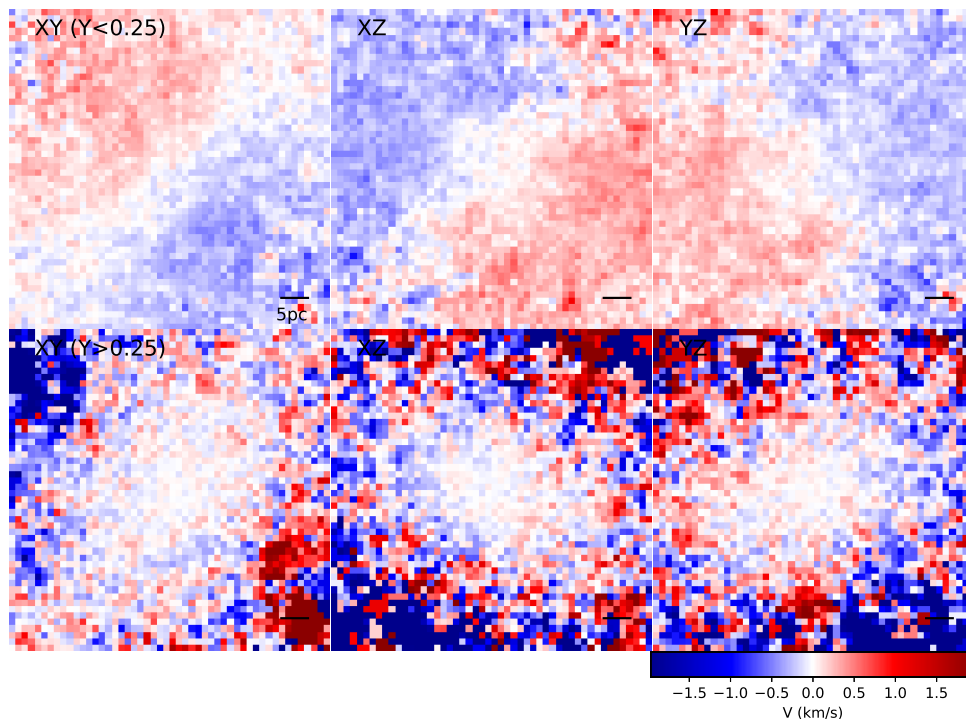


Fig. 2.— 2D kinematics of He-poor ($Y \leq 0.25$) and He-rich ($Y > 0.25$) stars for the three projections at the final time step in the fiducial model M1. The 2D map is based on the line-of-sight velocities (V_{los}) of stars within 30pc. For clarity, meshes with no He-rich particles are given the minimum value of V_{los} . Also, meshes with $V_{\text{los}} > 2 \text{ km s}^{-1}$ or $< -2 \text{ km s}^{-1}$ are given reddest and bluest colors, respectively, so that the color contrast between different regions can be more clearly seen.

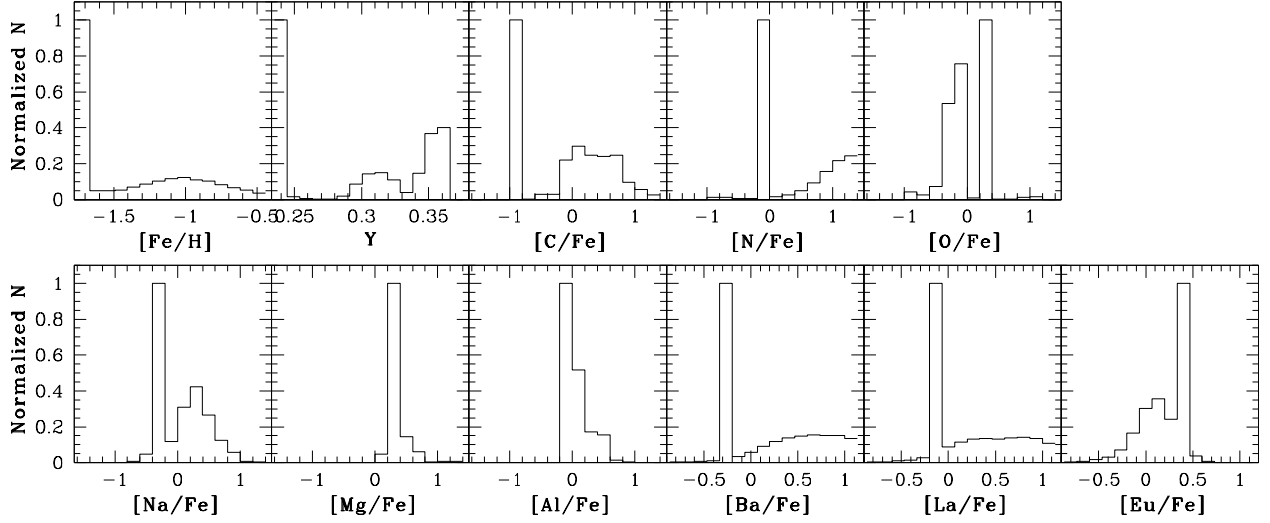


Fig. 3.— Abundance distribution functions (ADFs) of the 11 elements for the simulated ω Cen at the final time step in the fiducial model. For clarity, the number of stars in each bin is normalized by the maximum number of stars in the bins for each abundance. Only 30% of 1G stars are used for this analysis so that the ADFs of 1G and 2G stars can be clearly seen: if all 1G stars are used, then the distributions of 2G stars cannot be clearly seen owing to the dominant 1G population. As discussed in the main text, 1G stars are more efficiently stripped by the Galaxy during tidal interaction of ω Cen with the Galaxy owing to its more diffuse distribution. Therefore, removing a significant fraction of 1G stars in this analysis is physically reasonable. The location of the peak in the $[\text{C}/\text{Fe}]$ distribution (~ -1) reflects the adopted low initial carbon abundances of gas particles in the host GMC in this model. Therefore, this peak is not due to chemical enrichment processes during the GC formation (e.g., ejection of C-poor ejecta from AGB stars into ICM).

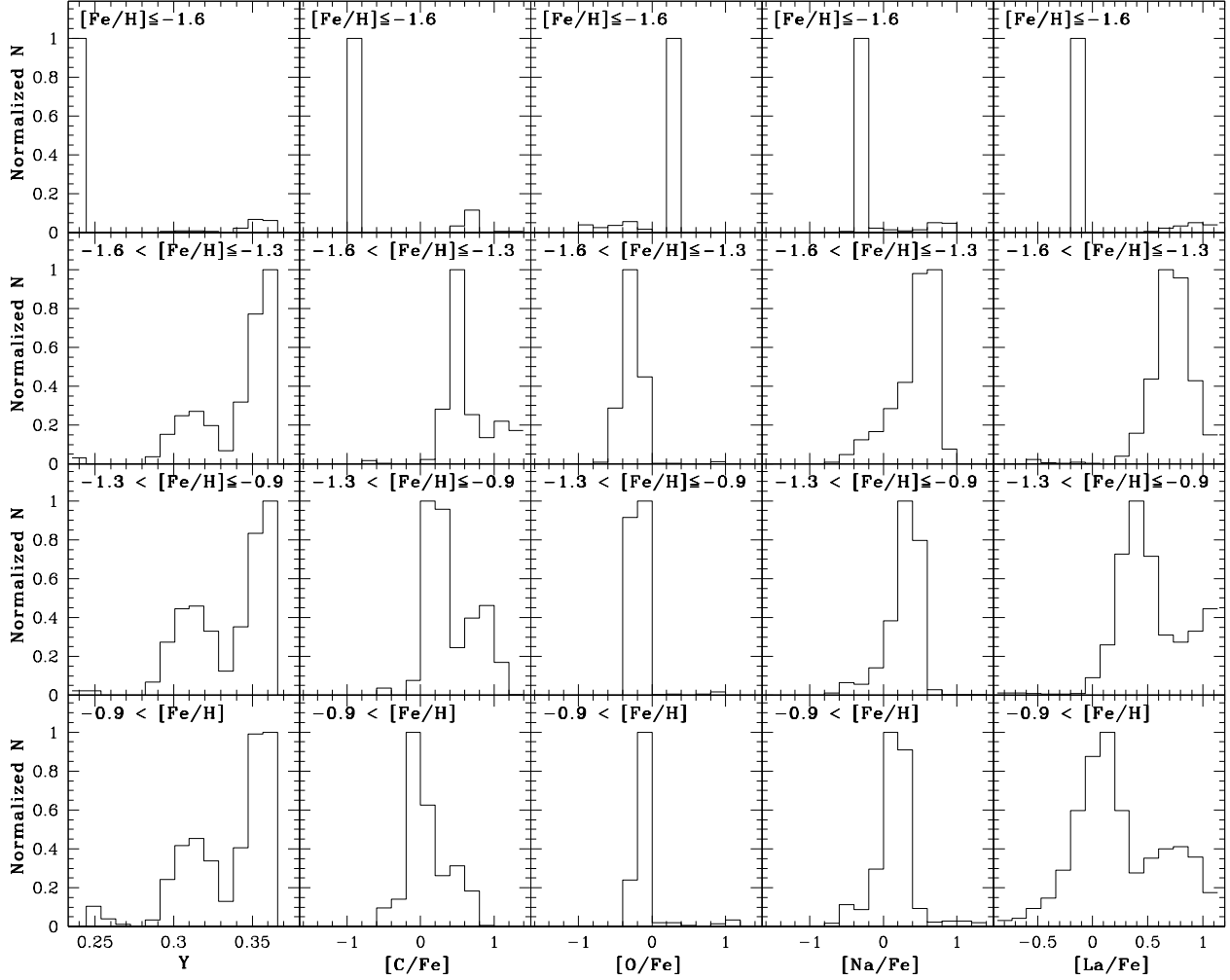


Fig. 4.— Abundance distribution functions of Y , $[\text{O}/\text{Fe}]$, $[\text{Na}/\text{Fe}]$, and $[\text{La}/\text{Fe}]$ for four different metallicity ranges in the simulated ω Cen at the final time step in the fiducial model M1. The metallicity ranges are chosen such that these results can be compared with observations by JP10.

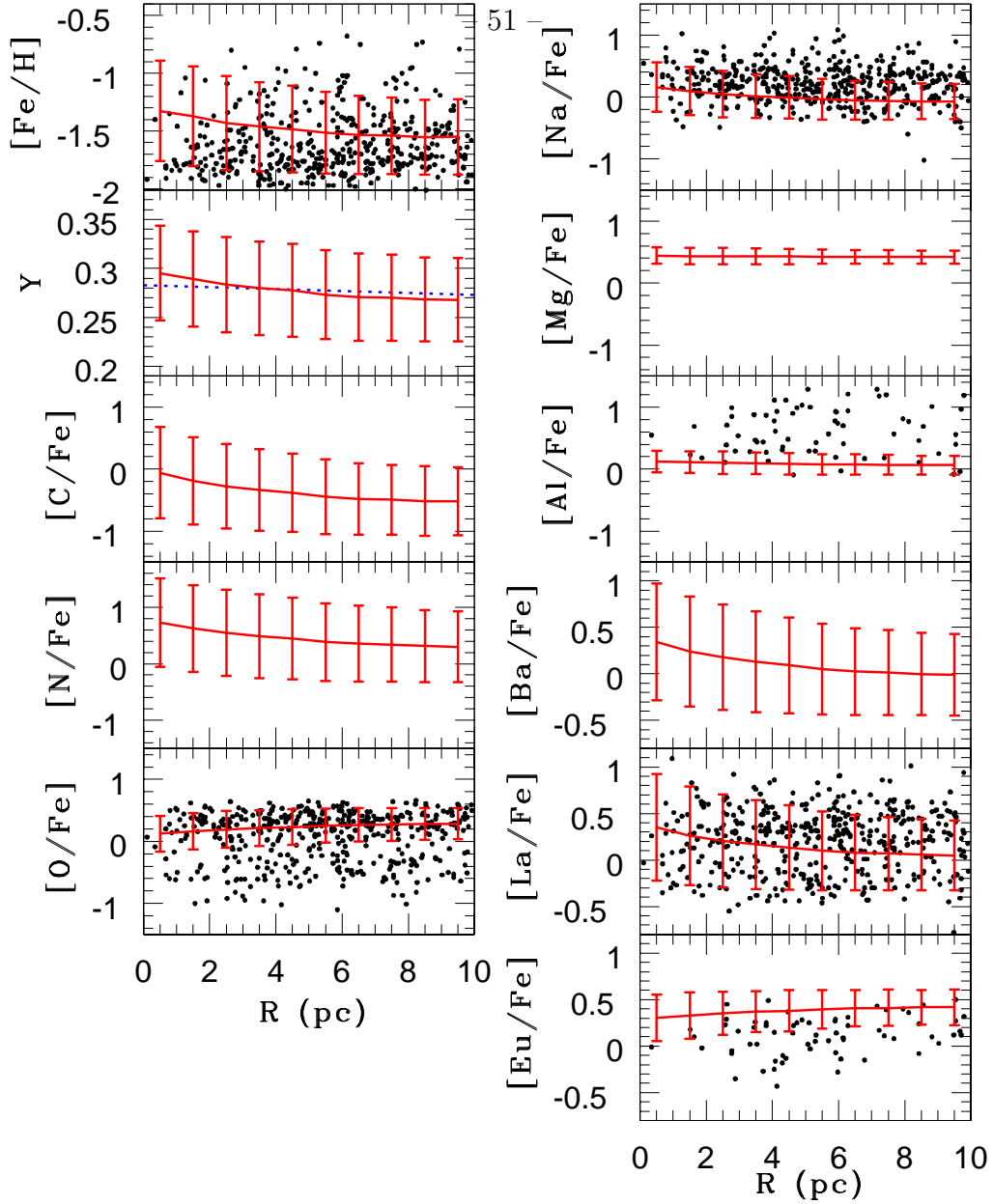


Fig. 5.— Radial gradients of the 11 elements in the simulated ω Cen at the final time step in the fiducial model M1 (red lines). The error bar shown in each radial bin for each abundance indicate the 1σ dispersion of the abundance. Black filled circles represent the observational results from JP10 and the blue dotted line for the radial gradient of Y is estimated from the observed radial profile of the number ratio (R_{bMS}) of blue main-sequence stars (“bMS”) to red main-sequence stars (“rMS”) by Sollima et al. (2007). Here Y is assumed to be 0.25 for rMS and 0.35 for bMS. The Y gradient is negative yet shallow (only 0.01 difference over 10 pc), though f_{bms} changes from 0.48 at $R = 0$ pc to 0.29 at $R = 10$ pc.

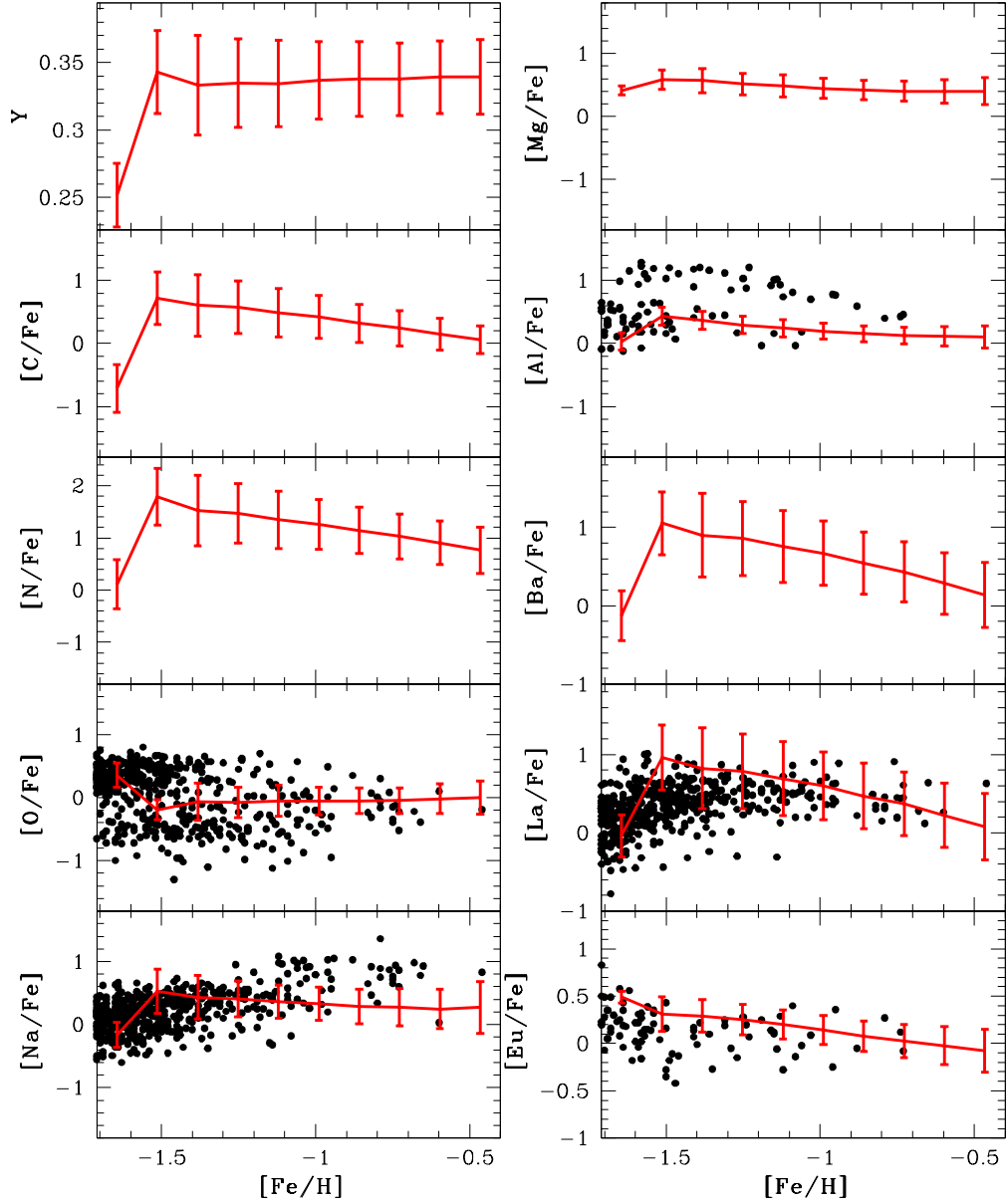


Fig. 6.— Relations between Y and $[\text{Fe}/\text{H}]$ and between $[\text{X}/\text{Fe}]$ and $[\text{Fe}/\text{H}]$, where $\text{X} = \text{C}, \text{N}, \text{O}, \text{Na}, \text{Mg}, \text{Al}, \text{Ba}, \text{La},$ and Eu , in the simulated ω Cen in the fiducial model M1 (red lines). The error bar shown in each $[\text{Fe}/\text{H}]$ bin for each abundance indicate the 1σ dispersion of the abundance. Black filled circles represent the observational results from JP10.

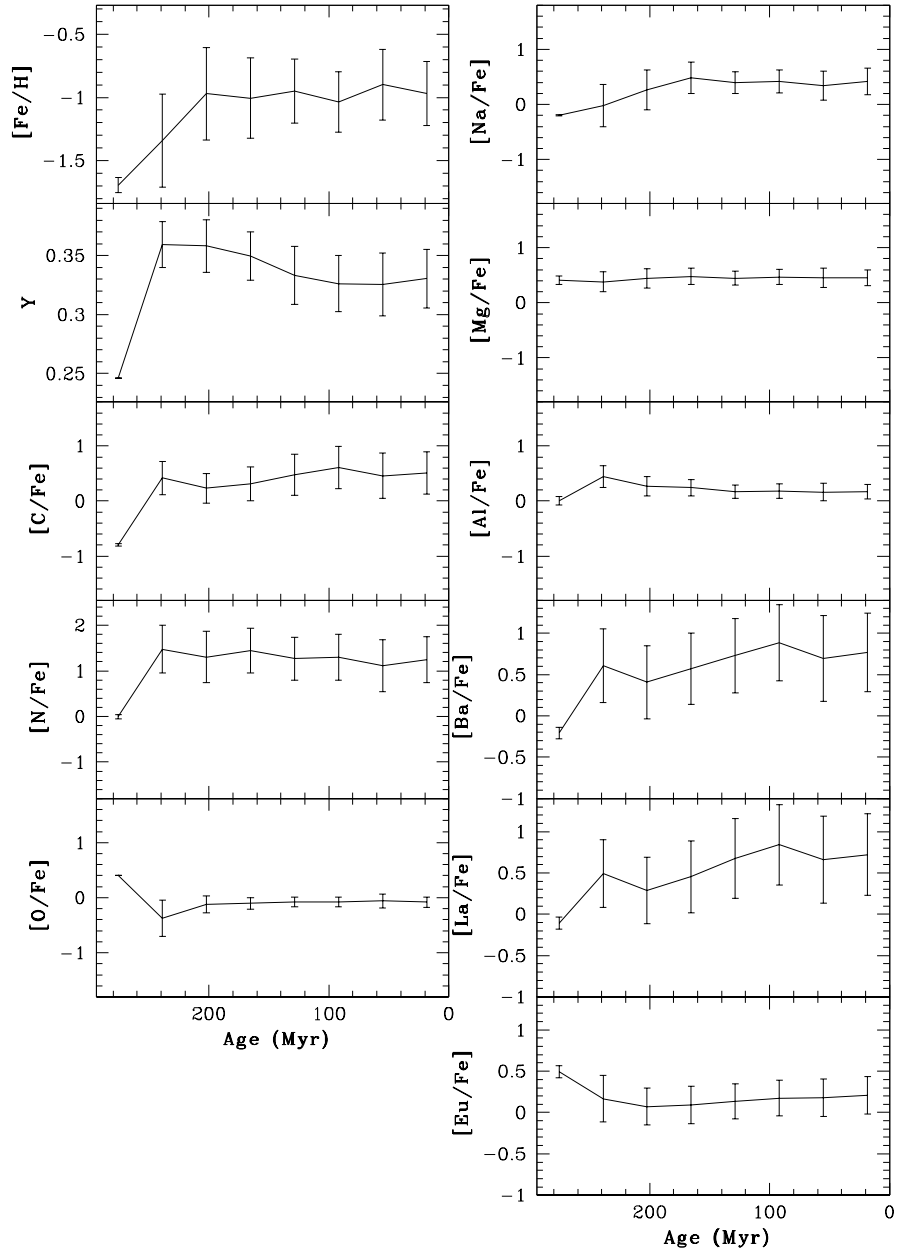


Fig. 7.— The age-abundance relation for the 11 elements in the simulated ω Cen in the fiducial model M1. The error bar shown in each age bin for each abundance indicate the 1σ dispersion of the abundance.

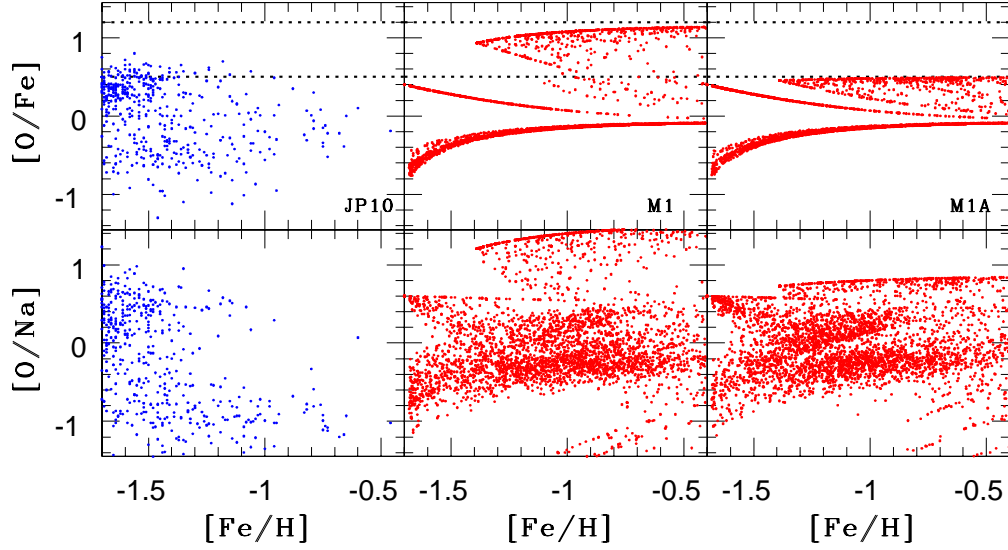


Fig. 8.— A comparison between the observed (blue, left) and simulated distributions (red, middle and right) of stars on the $[O/Fe]$ – $[Fe/H]$ (upper two) and $[O/Na]$ – $[Fe/H]$ planes (lower two). The fiducial model M1 and the comparative model M1A in which model parameters are exactly the same as M1 except for $[O/Fe]$ in the ejecta of massive SNe II. For convenience, only ≈ 4000 stars from simulated are selected and plotted. The adopted $[O/Fe]$ for massive SNe II are set to be 0.5 for $m \geq 15M_{\odot}$ in M1A. The yields of $[O/Fe]$ from K06 and Tominaga et al. (2007) are shown by upper and lower dotted lines, respectively, so that the results can be more clearly understood. The significant fraction of stars with high $[O/Fe]$ (> 1) for $[Fe/H] > -1.0$) is due to the adoption of yields from K06 in the present study.

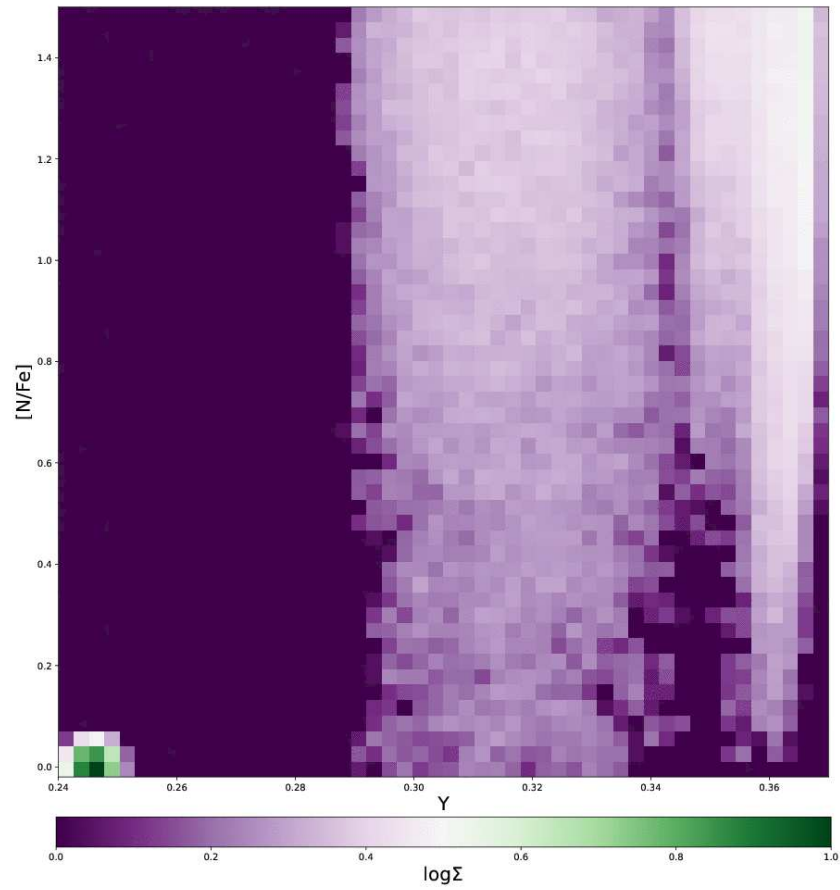


Fig. 9.— Distribution of stars on the Y - $[N/Fe]$ plane in the fiducial model. For clarity, the number density is normalized so that it can range from 0 to 1 in logarithmic scale. The highest density part at the lower left corner corresponds to the dominant 1G population. Three populations with different Y can be clearly seen in this map.

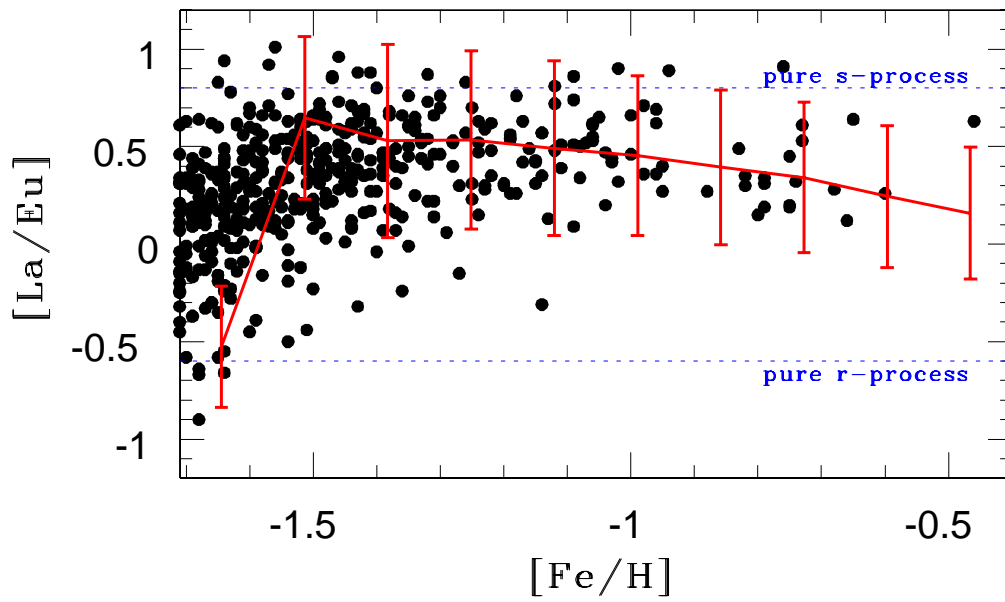


Fig. 10.— Evolution of $[La/Eu]$ with $[Fe/H]$ for the fiducial model, which can be compared with corresponding results from JP10 (e.g., their Figure 18). The abundance ratios for pure r - and s -process enrichment (Simmerer et al. 2004) are shown by dotted lines. Black filled circles represent the observational results from JP10.

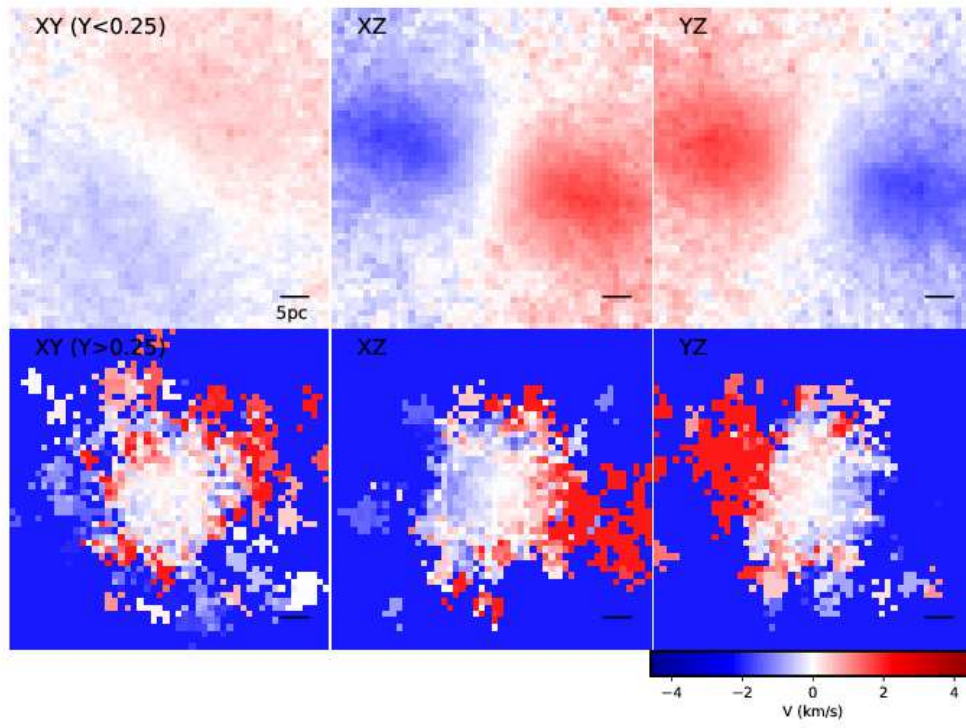


Fig. 11.— The same as Figure 2 but for the model M2 with $f_{\text{rot}} = 0.03$ (more initial angular momentum of the natal GMC).

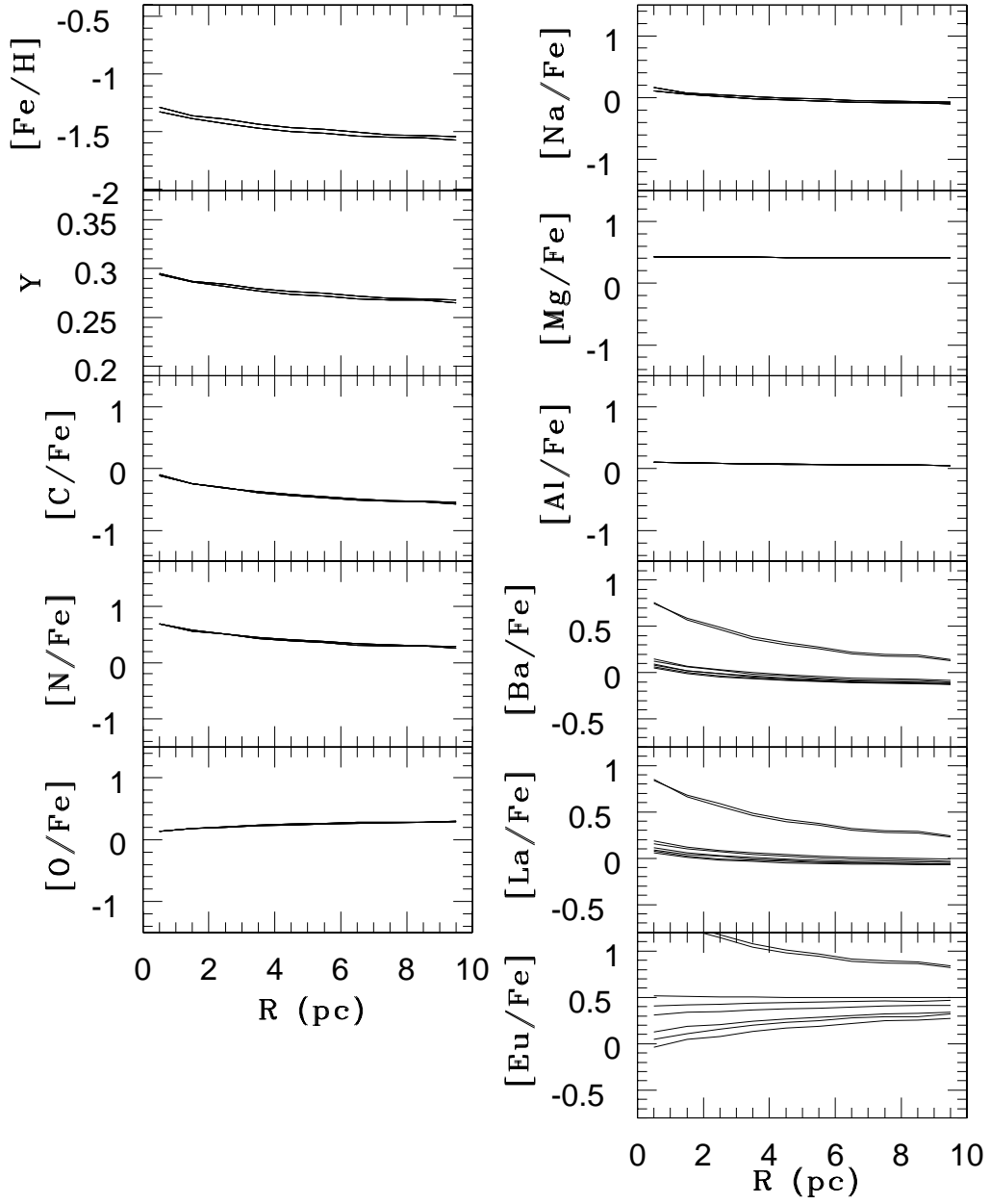


Fig. 12.— Radial gradients of the 11 elements for the representative 8 models with different mixing models (M2, M5, M6, M7, M8, M9, M11, and M12).

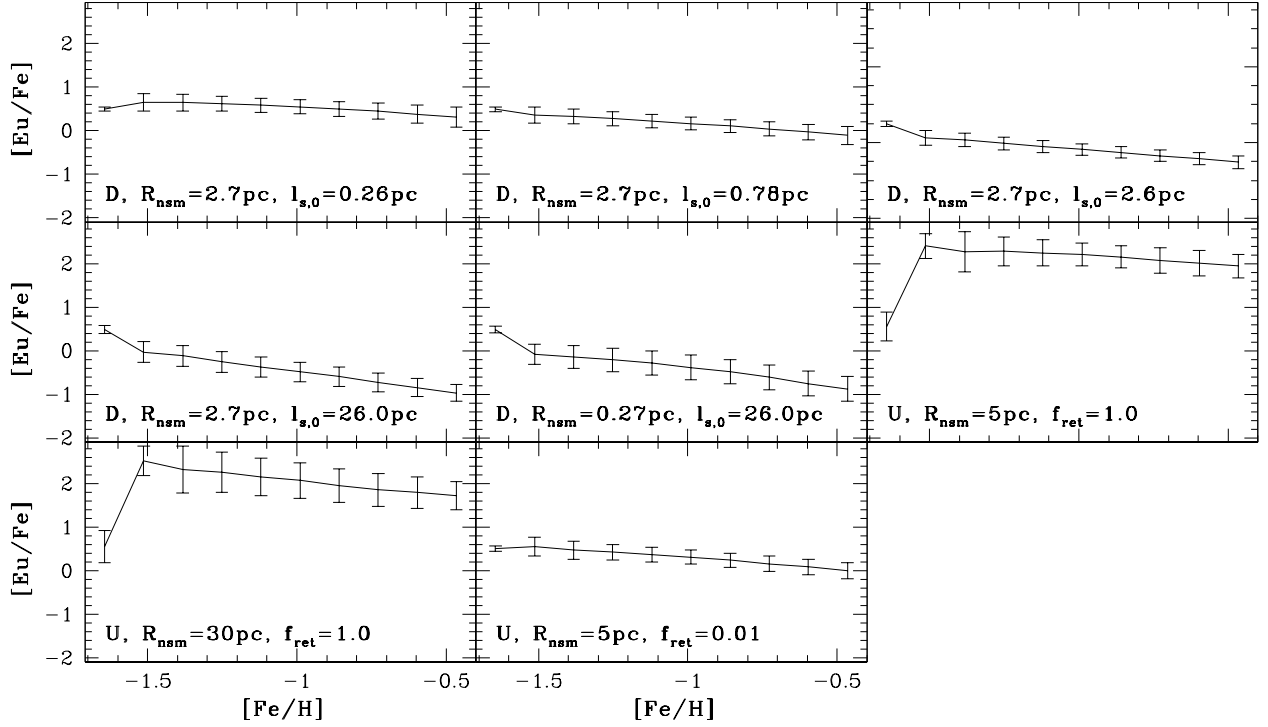


Fig. 13.— Evolution of $[\text{Eu}/\text{Fe}]$ with $[\text{Fe}/\text{H}]$ for 8 different mixing models (“D” or “U”) of NSM ejecta with different $r_{\text{ns}}m$ and $l_{s,0}$ (M2, M5, M6, M7, M8, M9, M11, and M12).

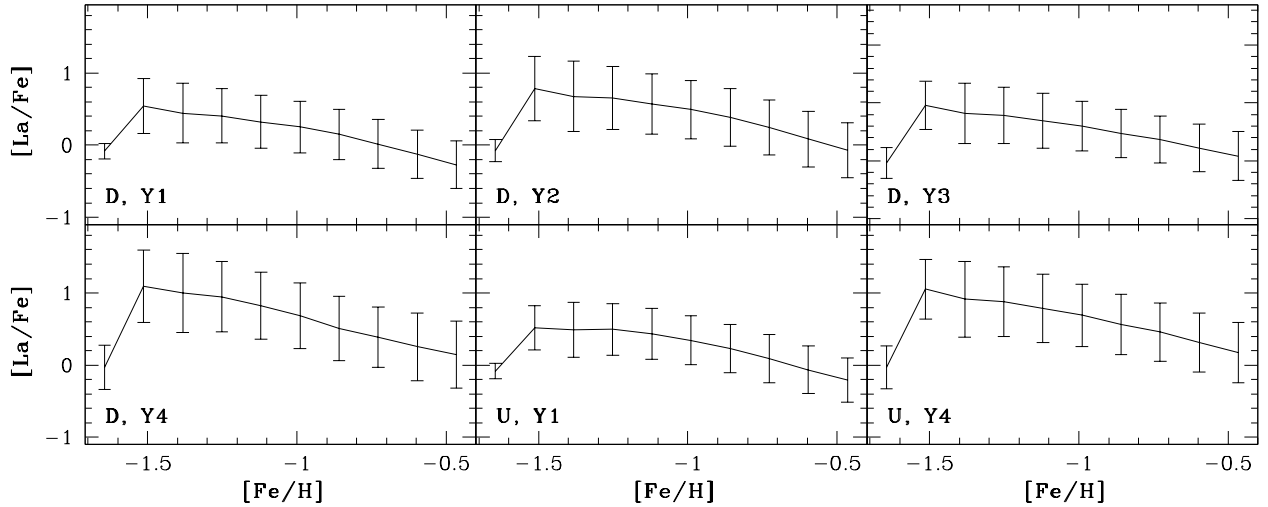


Fig. 14.— Evolution of $[\text{La}/\text{Fe}]$ with $[\text{Fe}/\text{H}]$ for 6 different mixing models with different AGB yields (M1, M2, M3, M4, M9, and M10).